Earth-Science Reviews 136 (2014) 155–174

Contents lists available at ScienceDirect

Earth-Science Reviews

journal homepage: www.elsevier.com/locate/earscirev

Australian sea levels—Trends, regional variability and influencing factors

Neil J. White [a,*], Ivan D. Haigh [b,c,d], John A. Church [a], Terry Koen [e], Christopher S. Watson [f], Tim R. Pritchard [e], Phil J. Watson [e], Reed J. Burgette [f,g], Kathleen L. McInnes [a], Zai-Jin You [h], Xuebin Zhang [a], Paul Tregoning [i]

[a] Centre for Australian Weather and Climate Research and Wealth from Oceans Flagship, CSIRO Marine and Atmospheric Research, Hobart, Tasmania, Australia
[b] Ocean and Earth Science, National Oceanography Centre, University of Southampton, European Way Southampton, UK
[c] School of Civil, Environmental and Mining Engineering, The University of Western Australia, M470, 35 Stirling Highway, Crawley, WA 6009, Australia
[d] Oceans Institute, University of Western Australia, Australia
[e] Office of Environment and Heritage, P.O. Box A290, Sydney South, NSW 1232, Australia
[f] School of Land and Food, University of Tasmania, Private Bag 76, Hobart, Tasmania 7001, Australia
[g] Department of Geological Sciences, New Mexico State University, Las Cruces, NM 88003, USA
[h] School of Civil Engineering, Ludong University, Yantai, China
[i] Research School of Earth Sciences, Australian National University, Canberra, ACT, Australia

ARTICLE INFO

Article history:
Received 7 October 2013
Accepted 17 May 2014
Available online 27 May 2014

Keywords:
Mean sea level
Land movements
Tide gauges
Altimetry data
Australia

ABSTRACT

There has been significant progress in describing and understanding global-mean sea-level rise, but the regional departures from this global-mean rise are more poorly described and understood. Here, we present a comprehensive analysis of Australian sea-level data from the 1880s to the present, including an assessment of satellite-altimeter data since 1993. Sea levels around the Australian coast are well sampled from 1966 to the present. The first Empirical Orthogonal Function (EOF) of data from 16 sites around the coast explains 69% of the variance, and is closely related to the El Niño Southern Oscillation (ENSO), with the strongest influence on the northern and western coasts. Removing the variability in this EOF correlated with the Southern Oscillation Index reduces the differences in the trends between locations. After the influence of ENSO is removed and allowing for the impact of Glacial Isostatic Adjustment (GIA) and atmospheric pressure effects, Australian mean sea-level trends are close to global-mean trends from 1966 to 2010, including an increase in the rate of rise in the early 1990s. Since 1993, there is good agreement between trends calculated from tide-gauge records and altimetry data, with some notable exceptions, some of which are related to localised vertical-land motions. For the periods 1966 to 2009 and 1993 to 2009, the average trends of relative sea level around the coastline are 1.4 ± 0.3 mm yr^{-1} and 4.5 ± 1.3 mm yr^{-1}, which become 1.6 ± 0.2 mm yr^{-1} and 2.7 ± 0.6 mm yr^{-1} after removal of the signal correlated with ENSO. After further correcting for GIA and changes in atmospheric pressure, the corresponding trends are 2.1 ± 0.2 mm yr^{-1} and 3.1 ± 0.6 mm yr^{-1}, comparable with the global-average rise over the same periods of 2.0 ± 0.3 mm yr^{-1} (from tide gauges) and 3.4 ± 0.4 mm yr^{-1} (from satellite altimeters). Given that past changes in Australian sea level are similar to global-mean changes over the last 45 years, it is likely that future changes over the 21st century will be consistent with global changes. A generalised additive model of Australia's two longest records (Fremantle and Sydney) reveals the presence of both linear and non-linear long-term sea-level trends, with both records showing larger rates of rise between 1920 and 1950, relatively stable mean sea levels between 1960 and 1990 and an increased rate of rise from the early 1990s.

Contents

* Corresponding author.
E-mail addresses: Neil.White@csiro.au (N.J. White), I.D.Haigh@soton.ac.uk (I.D. Haigh), John.Church@csiro.au (J.A. Church), Terry.Koen@environment.nsw.gov.au (T. Koen), Christopher.Watson@utas.edu.au (C.S. Watson), Tim.Pritchard@environment.nsw.gov.au (T.R. Pritchard), Phil.Watson@environment.nsw.gov.au (P.J. Watson), burgette@nmsu.edu (R.J. Burgette), Kathleen.Mcinnes@csiro.au (K.L. McInnes), b.you@ldu.edu.cn (Z.-J. You), Xuebin.Zhang@csiro.au (X. Zhang), paul.tregoning@anu.edu.au (P. Tregoning).

http://dx.doi.org/10.1016/j.earscirev.2014.05.011

1. Introduction

1.1. Overview

Sea-level change has become a major global scientific issue involving a wide range of disciplines (Church et al., 2010) with broad societal impacts (Nicholls and Cazenave, 2010). While there has been significant progress in describing (Douglas, 1991; Church et al., 2004; Church and White, 2006, 2011; Jevrejeva et al., 2006; Ray and Douglas, 2011) and understanding (Church et al., 2011a, 2013a; Moore et al., 2011; Church et al., 2013b; Gregory et al., 2013) global-mean sea-level (GMSL) rise, the regional departures from this global-mean rise are more poorly described and understood. The mean rate of GMSL rise over the 20th century was around 1.7 mm yr^{-1}, with an increase to around 3 mm yr^{-1} over the last 20 years (Church and White, 2011). Recent descriptions of local sea-level changes have been completed for a number of regions, some examples being studies of the North Sea (Wahl et al., 2013), British Isles (Woodworth et al., 2009), the English Channel (Haigh et al., 2009), the German Bight (Wahl et al., 2011), Norwegian and Russian coasts (Henry et al., 2012), the Mediterranean (Calafat and Jordà, 2011; Tsimplis et al., 2011, 2012), USA (Snay et al., 2007; Sallenger et al., 2012), and New Zealand (Hannah and Bell, 2012), the Indian Ocean (Han et al., 2010), Pacific Ocean (Merrifield et al., 2012) and Australia (Church et al., 2006). In this paper, we focus on describing and improving understanding of sea-level rise and variability around Australia, and its connection to variability in the surrounding oceans.

1.2. Previous analyses

Gehrels et al. (2012) used sea levels recorded in salt marsh sediments to infer sea level was stable in the Tasmanian and New Zealand region, at about 0.3 m lower than at present, through the middle and late Holocene up to the late 19th century. The rate of sea-level rise then increased in the late 19th century, resulting in a 20th century average rate of relative sea-level rise in eastern Tasmania of 1.5 ± 0.4 mm yr^{-1}. This, and other analyses (e.g. Lambeck, 2002; Gehrels and Woodworth, 2013) suggest an increase in the rate of global and regional sea-level rise in the late 19th and/or the early 20th Centuries. The earliest known direct measurements of sea level in Australia are from a two-year record (1841–1842) at Port Arthur, Tasmania relative to an 1841 benchmark (Hunter et al., 2003). Hunter et al. (2003) estimated a sea-level rise over the 159 years to 1999–2002 of 0.135 m (at an average rate of 0.8 mm yr^{-1}). If, following Gehrels et al. (2012), most of this rise occurred after 1890, the 20th century rate would be 1.3 mm yr^{-1}, or 1.5 mm yr^{-1} after correction for land uplift (Hunter et al., 2003 and Hunter pers comm).

Recent analyses extend to studies involving the two long near-continuous tide-gauge records; on the East coast at Sydney (Fort Denison, 1886–), and on the west coast Fremantle (1897–). You et al. (2009) estimated rates of relative sea level rise at Fort Denison of 0.63 ± 0.14 mm yr^{-1} for 1886–2007, 0.93 ± 0.20 mm yr^{-1} for 1914–2007 and 0.58 ± 0.38 mm yr^{-1} for 1950–2007. Mitchell et al. (2000) estimated a trend of 0.86 mm yr^{-1} for 1914–1997. For Fremantle, Haigh et al. (2011) found rates of relative sea level rise of 1.46 ± 0.15 mm yr^{-1} for the period 1897–2008, −0.54 ± 2.42 mm yr^{-1} for 1967–1990, 1.71 ± 0.68 mm yr^{-1} for 1967–2008, and 5.66 ± 2.90 mm yr^{-1} for 1992–2008. Other long running sites (e.g. Williamstown and Port Adelaide Inner Harbour) have not been useful for determining long-term trends because of deficiencies, including large gaps and/or datum shifts for Williamstown, and land subsidence for Port Adelaide. The Newcastle records also have problems with subsidence (Watson, 2011). In general, individual Australian tide-gauge records are too short and contain too much variability for detection of statistically significant accelerations or decelerations in sea-level rise.

In a companion paper to the present study, Burgette et al. (2013) used a network adjustment approach to mitigate inter-annual and decadal variability, estimating weighted average linear rates of sea-level change relative to the land (trend ± 1 standard error) of 1.4 ± 0.6, 1.7 ± 0.6 and 4.6 ± 0.8 mm yr^{-1}, over three temporal windows including the altimeter era: 1900–2011; 1966–2011; and 1993–2011 respectively. Similar spatial patterns in rates of sea-level change were observed, with the highest rates present in Northern Australia. Burgette et al. (2013) also showed that time-series variability (noise with respect to a linear model) changes spatially, best described by a first-order Gauss–Markov model in the west, whilst east coast stations were better described by a power-law process.

Aubrey and Emery (1986) estimated an average relative sea-level rise of 1.3 mm yr^{-1} from 25 Australian tide-gauge records with length varying from as little as 11 years to as much as 87 years. They ascribed the sea-level rise in the south-east and the sea-level fall in the north to differential land motion. Bryant et al. (1988) pointed out that this spatial variability was mainly due to climatic, not geological, signals. Mitchell and Lennon (1992) found a median value of relative rise of 1 mm yr^{-1} and an average of 1.51 ± 0.18 mm yr^{-1} (95% confidence interval) for 39 Australian Records, the shortest having a length of about 11 years. Amin (1993) estimated an average rate of rise of 1.7 mm yr^{-1} using data from just four ports on the west and north-west coast of Australia (Fremantle, Geraldton, Wyndham and Darwin) for the 21-year period from 1966 to 1986. Church et al. (2006) estimated a relative sea-level trend averaged around Australia of 1.2 mm yr^{-1} from 1920 to 2000. Haigh et al. (2011) analysed data from 14 tide gauges around Western Australia. They concluded that

the Fremantle record indicated a rate of rise comparable with estimates of global mean change, and that in southern Western Australia the rate of MSL rise was less than the global average, but that it was greater than the global average in northern Western Australia. For the period of high-quality satellite-altimeter data (since 1993), sea levels around Australia have been rising at close to the global average (about 3 mm yr^{-1}) in the south and south-east and above the global average in the north and north-west (Deng et al., 2011; Haigh et al., 2011).

Multiple studies (Pariwono et al., 1986; Amin, 1993; Church et al., 2004; Feng et al., 2004; Church et al., 2006; Haigh et al., 2011) all identified inter-annual and decadal sea-level variability related to ENSO on the west, south-west and south coasts of Australia. In particular, Feng et al. (2004), Church et al. (2006) and Haigh et al. (2011) showed that sea level rose rapidly in the 1920s and 1940s and again in the 1990s at Fremantle, but was relatively stable between 1970 and 1990. These studies also noted that the multidecadal variations in Fremantle sea level were related to climate variability in the tropical Pacific as characterised by the Southern Oscillation Index (SOI). Haigh et al. (2011) found the strength of the correlation of Fremantle sea level and the SOI was not constant in time and that the variability in sea level around the Western Australian coast was weakly negatively correlated to the Indian Ocean Dipole (IOD) index and weakly positively correlated to the Southern Annular Mode (SAM) for the period 1967–2008. For the Pacific and Indian Oceans, Zhang and Church (2012) showed that, for the satellite altimeter data since 1993, a multiple linear regression of sea level on time, a Multivariate ENSO Index and the Pacific Decadal Oscillation explained more of the variance than a linear regression on time only. However, there was low skill in the Tasman Sea, consistent with a several year lag between the Interdecadal Pacific Oscillation and low frequency sea level at Sydney (Holbrook et al., 2011).

1.3. Aims and structure

In this paper, we present a comprehensive analysis of Australian sea-level data from the 1880s to the present, with a focus on understanding and quantifying the long-term trends and the influence of inter-annual and decadal variability, and correlations of this variability with climate indices. We also consider the effects of changes in atmospheric pressure (the inverse barometer effect, Wunsch and Stammer, 1997), as well as vertical land motion (VLM).

When discussing trends, the quantity of most interest to coastal managers, engineers and planners, is the rate of mean sea-level rise relative to the land, referred to herein as relative mean sea level (RMSL). Our analysis is focussed on changes in RMSL determined using monthly means of tide gauge measurements, each of which are observed relative to the land supporting the tide gauge. Estimates of RMSL change are not directly comparable to measurements of sea level made from satellite altimetry, which by definition are made with respect to an Earth-fixed geocentric reference frame, hereon termed *geocentric MSL*. Comparison and interpretation of relative and geocentric MSL requires understanding of ongoing vertical land motion (VLM) and its influence on sea level observed over all spatial scales from point locations to across the global oceans. In this context, we introduce *ocean-volume* MSL (OVMSL) as a measure of change in the volume of water in the oceans, corrected for the various effects of VLM, including changes in the Earth's gravity field (geoid) and shape of the ocean basins. We define in detail relative, geocentric and ocean-volume MSL in Section 2.3.

We commence with a review of data sets and reference frames (Section 2), before investigating the characteristics of inter-annual and decadal variability in the sea-level data (Section 3). Sea-level trend estimates are presented (Sections 3 & 4) then discussed (Section 5) and finally conclusions are given (Section 6).

2. Data sets

2.1. Tide-gauge records

Tide-gauge measurements of sea level began in the 18th century with visual observations of the heights of high and low waters at a few locations (mostly in Europe). By the 1830s automatic float tide gauges had been developed that could record the full tidal curve and by the end of the 19th century these had been installed at most major ports around the world (Woodworth et al., 2011). The observations were originally designed to support port operations and navigation. In Australia, they were also used to determine the Australian Height Datum (AHD) using data from 1966 to 1968 from 30 tide gauges (Featherstone and Filmer, 2012).

Our analysis focuses predominantly on monthly mean data from the Permanent Service for Mean Sea Level (PSMSL; Woodworth and Player, 2003; PSMSL, 2012). Data are available for more than 2000 gauges around the world in the form of both monthly and annual (derived from the monthly values) RMSL. However, there is a paucity of long southern hemisphere tide-gauge records; only two of 123 records held by the PSMSL which pre-date 1900 are located in the southern hemisphere, the two longest records being Sydney (Fort Denison) from 1886 and Fremantle from 1897.

The data available from the PSMSL are designated either 'Metric Data' or 'Revised Local Reference' (RLR) data. Many Metric records have large discontinuities from one section of data to the next. For RLR records, sufficient levelling information is available to unambiguously join a number of sections into one continuous record (relative to a common benchmark) suitable for analysis of long-term trends. Thus, the RLR records are preferred for trend analysis. However, some of the RLR records still have problems due to localised VLM (e.g. wharf instability or local subsidence), and some of the longer Metric records are usable for long-term analysis due to their continuous nature.

The Australian National Tidal Centre (NTC), which is now part of the Australian Bureau of Meteorology, collects data from several state organisations and port authorities who operate tide gauges around the coast of Australia and provide monthly MSL values to the PSMSL. The NTC also maintains a national network of 16 tide gauges around Australia as part of the Australian Base Line Sea Level Monitoring Network (ABSLMP). This array of SEAFRAME (SEA-level Fine Resolution Acoustic Measuring Equipment) tide gauges was installed between 1991 and 1993.

The PSMSL's RLR and Metric subsets contain 81 records from 76 sites and 215 records from 139 sites from around the coast of Australia, respectively. We focus on the RLR dataset, but exclude records with less than 15 years of data. At Newcastle and Sydney (Fort Denison), different records were combined to form single longer time series at each site (see supplementary material for details). After careful consideration, we supplemented this RLR dataset with records from the Metric set. In some cases, we replaced RLR records with the equivalent Metric record where these were longer and free from datum issues.

Our final dataset comprises records at 69 sites (Fig. 1, Table 1). In addition to the PSMSL quality control procedures, each record was compared to the time series from neighbouring sites and to a 'MSL index', that represents the coherent part of the MSL variability around Australia (see Section 3). This MSL index was created, following a method described in Woodworth et al. (2009), Haigh et al. (2009) and Wahl et al. (2013), by: de-trending each of the time series using linear regression over their whole record length; and then, for each year, averaging all of the MSL values available for that year. Using this method, we were able to identify values which deviated significantly from this index. The values (1% of the data set) were then excluded from the analysis. A detailed list of the acceptable records as well as the suspect values excluded from the analysis, along with figures showing the comparison of each record with time series from neighbouring sites and the MSL index, is given in the supplementary material. In addition, if, for any calendar year of any record, there are

less than 11 good monthly values, all values for that year and record are rejected.

A graphical comparison of yearly averaged RMSL from the Australian tide gauges with globally averaged GMSL from Church and White (2011) may be undertaken by first expressing both datasets as OVMSL (Fig. 2a, see Section 2.3 for detail on corrections required to generate OVMSL—note that the Church and White (2011) GMSL is already in the sense of OVMSL). For this comparison, the 1971–2000 mean was first removed from the GMSL time series (already expressed in the sense of ocean-volume). Tide-gauge time series were then added following conversion from RSL to OVMSL using GIA (but not GPS VLM) data and removal of mean differences with respect to the GMSL series over whatever common years they had in the 1971–2000 (inclusive) time span. This time span was chosen because it is the earliest 30-year period for which all tide-gauge records have sufficient data. The records flagged because of possible ground movement and credibility issues are not used in calculating averages, but are shown on Fig. 2a for comparison. It is clear these suspect gauges deviate significantly from the majority of tide-gauge records and the GMSL time series. Since 1920, OVMSL around the Australian coast approximately follows the global mean over longer (multi-decadal) time periods, but with substantial excursions from the long-term mean due to inter-annual and decadal variability (Fig. 2a). For example, Australian MSL rose slightly faster than the global average from 1920 to 1950, slower than the global average from about 1960 to 1990, and similar to the global average since about 1990. Note the clearly coherent signals (such as the falls in sea level during the 1983, 1986 and 1997 El Niño events). Fig. 2b is similar, except that signals correlated with ENSO (as characterised by the Southern Oscillation Index—SOI) have been removed from the Australian tide-gauge data that is displayed, as will be discussed in detail in Sections 3 and 4.

2.2. Altimeter data

Satellite altimeters have provided high quality, near-global measurements of sea-surface height (SSH) since 1993. Altimeter derived SSH data at 1 Hz (~7 km along-track) has an accuracy of ~2–3 cm with respect to an Earth-fixed reference frame (Fu and Cazenave, 2001). Local, regional or global means of altimeter SSH may be expressed as geocentric or OVMSL (see Section 2.3). Here, we use data from the TOPEX/Poseidon (1993–2002), Jason-1 (2002–2009) and OSTM/Jason-2 (2008–2011) satellite altimeter missions (the years in brackets indicating the years of data used from each mission) that measure SSH from 66°S to 66°N every ~10 days. The dataset used in this paper has been mapped to a 1° × 1° grid and averaged into monthly values (see Church and White, 2011, Chapter 1 of Fu and Cazenave, 2001, http://www.cmar.csiro.au/sealevel/sl_meas_sat_alt.html and http://www.altimetry.info/ for further detail).

The satellite altimeter data uses orbits referenced to ITRF2008, and has (as far as possible) consistent corrections for path delays (dry troposphere, wet troposphere, ionosphere), surface wave effects (sea-state bias) and ocean tides. There is no adjustment to agree with tide gauge data. See Fu and Cazenave (2001), Church and White (2011) for more detail. Note that the altimeter processing has been upgraded since Church and White (2011) and, apart from the improved corrections, there is now no calibration against tide gauges for any of the missions.

2.3. Reference frames and vertical land movements

In order to place locally observed trends in relative MSL (RMSL, the focus of this paper), into a regional or global context and compare with observations from satellite altimetry, we need to consider the different reference frames in use and account for the effects of VLM.

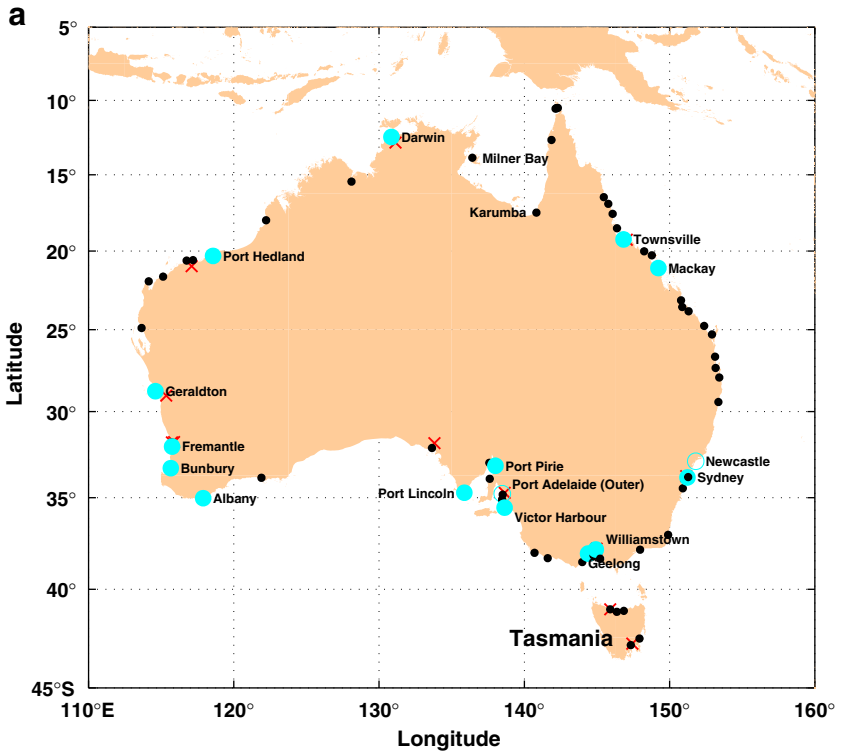

Fig. 1. (a): Tide-gauge locations (black and cyan dots) and GPS sites (crosses) used in this study. The lengths of the records are indicated in Fig. 1(b). Bars on Fig. 1(b) start at Milner Bay and go anti-clockwise around the coastline to Karumba with a diversion to Tasmania. The 16 gauges used in section 3 and table 4 are shown as cyan dots and named. The gauges used in section 3 are named and shown as cyan dots. The open cyan circles indicate the gauges used for variability, but not trends in Section 3. (b): Data spans for records used in the study are shown by the bars, blue for RLR records and red for Metric records. Small unusable fragments have been removed as described in the text. The '(A)' annotations after the names indicate that the record is at least partly an ABSLMP array.

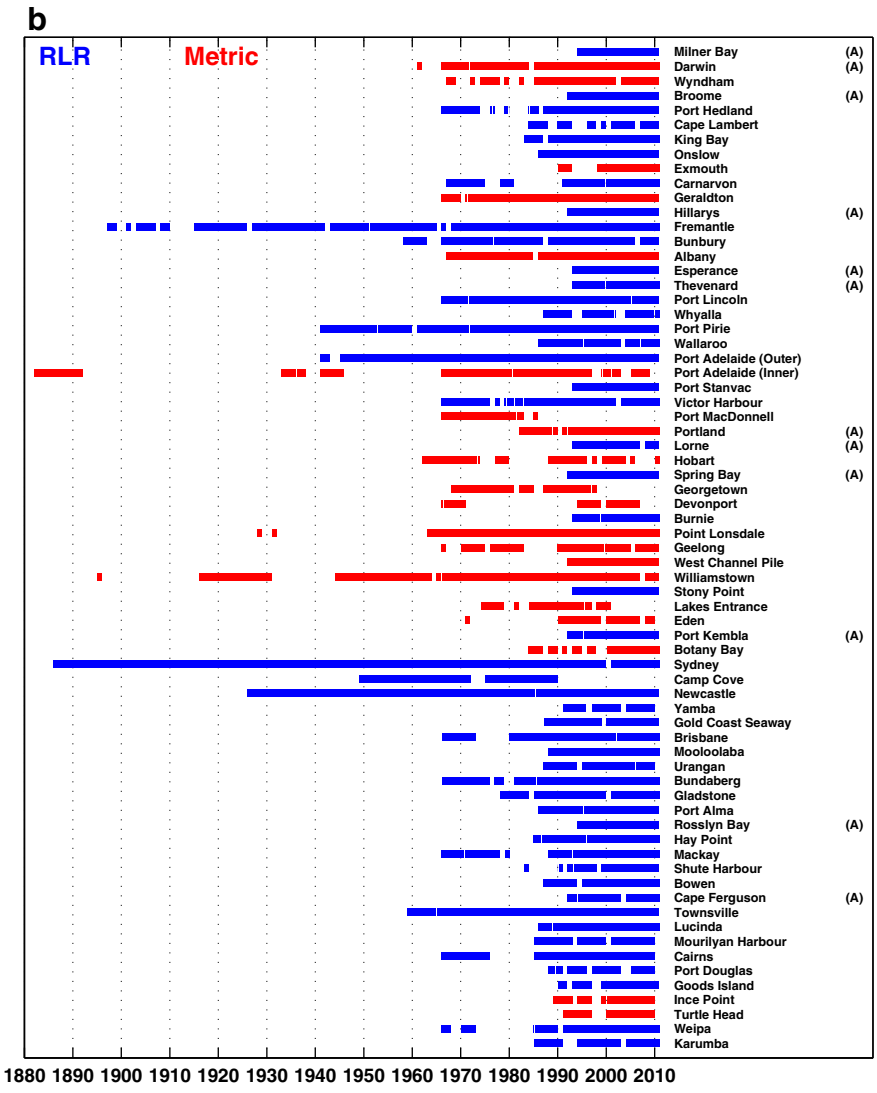

Fig. 1 (*continued*).

Vertical movement of the Earth's surface is driven by a range of geophysical processes operating over various spatial and temporal scales, such as crustal deformation induced by earthquakes, uplift/subsidence caused by changes in loads on the Earth's crust through the accumulation or extraction of ground water or oil and the on-going elastic and visco-elastic response of the crust to changes in present and past ice mass loads, known as Glacial Isostatic Adjustment (GIA). GIA models combine information describing the evolution of ice extent (and volume) over the Earth's surface with information describing the internal Earth structure to derive several quantities of interest for sea level studies. As part of these computations, changes in the rotational behaviour of the Earth caused by the associated mass redistributions introduce a feedback that is considered with the model. For our purposes, the model outputs of significance are

a) vertical velocity of the crust (including the continent surface and ocean floor),
b) vertical velocity of the sea surface (the "geoid" in GIA terminology, Tamisiea, 2011; Tamisiea and Mitrovica, 2011).

Derived from a) and b) is c) the vertical rate of change of the thickness of the water envelope. The later item (c) is usually referred to as relative sea-level change due to GIA and is normally used for correcting tide-gauge data, while term b) is normally used for correcting satellite altimeter data (Tamisiea, 2011; Tamisiea and Mitrovica, 2011).

Localised VLM in the vicinity of a tide gauge caused by ground water extraction for example, has a direct and obvious effect on measurements of RMSL. More subtly, the GIA component of VLM will induce changes in the Earth's gravity field (geoid) as well as in the shape (and hence volume) of the ocean basins (Tamisiea and Mitrovica, 2011). Both of these changes influence relative and geocentric MSL dictating that a small correction is required in order to infer changes in ocean volume (the most useful measure for understanding the physical reasons for MSL change). When considering global averages derived from satellite altimetry, GIA related effects that induce changes in seafloor position and variation in the gravity field will contribute -0.15 mm yr^{-1} to -0.5 mm yr^{-1} to changes in geocentric GMSL (Tamisiea, 2011), with the range reflecting variability in available Earth and ice models used in modeling GIA. Models of GIA are therefore required to remove these effects from RMSL (at tide gauges) and geocentric MSL (from altimetry) to yield estimates in the sense of OVMSL. The GIA correction applied to the altimeter data is spatially varying, rather than a global-mean value as is often used for global studies.

The nomenclature surrounding GIA and MSL is often confusing across the oceanographic, geodetic and GIA modelling literature. The terms geocentric and absolute MSL have been used interchangeably in much of the GIA and geodetic literature (e.g. Wöppelmann et al., 2009; Tamisiea, 2011; King et al., 2012). Here, we prefer to use only the term geocentric MSL, defined as the measurement of MSL relative

Table 1
Summary of useable tide-gauge data. Columns from left to right are (1) name as in the PSMSL archive, (2) shorter version of the name, (3) PSMSL id, (4) RLR or Metric (see Section 2), (5) is this an ABSLMP station, (6) latitude, (7) longitude, (8) first and (9) last year of useable data as defined in the text, (10) used for Trends (T), Variability (V) or not at all (X), (11) comments.

PSMSL name	Short name	PSMSL id	RLR/Metric	ABSLMP?	Lat	Long	Start	End	T/V/X?	Comment
MILNER BAY (GROOTE EYLANDT)	Milner Bay	1160	RLR	Yes	−13.86	136.42	1994	2010	TV	
DARWIN	Darwin	935	Metric	Yes	−12.47	130.85	1961	2010	TV	
WYNDHAM	Wyndham	1116	Metric		−15.45	128.10	1967	2010	X	See text
BROOME	Broome	1159	RLR	Yes	−18.00	122.22	1992	2010	TV	
PORT HEDLAND	Port Hedland	189	RLR		−20.32	118.57	1966	2010	TV	
CAPE LAMBERT	Cape Lambert	1328	RLR		−20.59	117.19	1984	2010	X	Insufficient data
KING BAY	King Bay	1549	RLR		−20.62	116.75	1983	2010	TV	
ONSLOW	Onslow	1631	RLR		−21.65	115.13	1986	2010	TV	
EXMOUTH	Exmouth	1762	Metric		−21.95	114.14	1990	2010	X	Insufficient data
CARNARVON	Carnarvon	1115	RLR		−24.90	113.65	1967	2010	TV	
GERALDTON	Geraldton	1031	Metric		−28.78	114.60	1966	2010	TV	
HILLARYS	Hillarys	1761	RLR	Yes	−31.83	115.74	1992	2010	X	See text
FREMANTLE	Fremantle	111	RLR		−32.07	115.75	1897	2010	TV	
BUNBURY	Bunbury	834	RLR		−33.32	115.66	1958	2010	TV	
ALBANY	Albany	957	Metric		−35.03	117.89	1967	2010	TV	
ESPERANCE	Esperance	1114	RLR	Yes	−33.87	121.90	1993	2010	TV	
THEVENARD	Thevenard	386	RLR	Yes	−32.15	133.64	1993	2010	TV	
PORT LINCOLN	Port Lincoln	230	RLR		−34.72	135.87	1966	2010	TV	
WHYALLA III	Whyalla	1367	RLR		−33.01	137.59	1987	2010	TV	
PORT PIRIE	Port Pirie	216	RLR		−33.18	138.01	1941	2010	TV	
WALLAROO II	Wallaroo	1420	RLR		−33.93	137.62	1983	2010	TV	
PORT ADELAIDE (OUTER HARBOR)	Port Adelaide (Outer)	448	RLR		−34.78	138.48	1941	2010	V	Belperio (1993)
PORT ADELAIDE (INNER HARBOR)	Port Adelaide (Inner)	50	Metric		−34.83	138.51	1882	2008	X	Belperio (1993)
PORT STANVAC	Port Stanvac	1506	RLR		−35.11	138.47	1993	2010	TV	
VICTOR HARBOUR	Victor Harbour	1069	RLR		−35.56	138.64	1966	2010	TV	
PORT MACDONNELL II	Port MacDonnell	1178	Metric		−38.05	140.70	1966	1985	TV	
PORTLAND	Portland	1547	Metric	Yes	−38.34	141.61	1982	2010	TV	
LORNE	Lorne	1836	RLR	Yes	−38.55	143.99	1993	2010	TV	
HOBART	Hobart	838	Metric		−42.88	147.33	1958	2010	X	Insufficient data
SPRING BAY	Spring Bay	1216	RLR	Yes	−42.55	147.93	1992	2010	TV	
GEORGETOWN	Georgetown	1120	Metric		−41.13	146.85	1968	2005	TV	
DEVONPORT	Devonport	1118	Metric		−41.18	146.37	1966	2006	X	Insufficient data
BURNIE	Burnie	683	RLR		−41.05	145.91	1993	2010	TV	
POINT LONSDALE	Point Lonsdale	301	Metric		−38.29	144.61	1928	2010	X	See text
GEELONG	Geelong	1117	Metric		−38.09	144.39	1966	2010	TV	
WEST CHANNEL PILE	West Channel Pile	1778	Metric		−38.19	144.76	1992	2010	TV	
WILLIAMSTOWN	Williamstown	93	Metric		−37.87	144.92	1895	2010	TV	
STONY POINT	Stony Point	1033	RLR		−38.37	145.22	1993	2010	TV	
LAKES ENTRANCE	Lakes Entrance	1379	Metric		−37.88	147.97	1974	2010	TV	
EDEN	Eden	833	Metric		−37.07	149.90	1971	2009	TV	
PORT KEMBLA	Port Kembla	831	RLR	Yes	−34.47	150.91	1992	2010	TV	
BOTANY BAY	Botany Bay	1525	Metric		−33.98	151.22	1984	2010	TV	
SYDNEY	Sydney	65	RLR		−33.85	151.23	1886	2010	TV	
CAMP COVE	Camp Cove	549	RLR		−33.83	151.28	1949	1989	TV	
NEWCASTLE III	Newcastle	267	RLR		−32.92	151.80	1926	2010	V	See text
YAMBA	Yamba	310	RLR		−29.43	153.36	1991	2009	TV	
GOLD COAST SEAWAY 2	Gold Coast Seaway	1704	RLR		−27.95	153.42	1987	2010	X	See text
BRISBANE (WEST INNER BAR)	Brisbane	822	RLR		−27.37	153.17	1966	2010	TV	
MOOLOOLABA 2	Mooloolaba	1493	RLR		−26.68	153.13	1988	2010	TV	
URANGAN	Urangan	2073	RLR		−25.30	152.92	1987	2009	TV	
BUNDABERG	Bundaberg	1154	RLR		−24.77	152.38	1966	2010	TV	
GLADSTONE	Gladstone	825	RLR		−23.85	151.31	1978	2010	TV	
PORT ALMA	Port Alma	2072	RLR		−23.58	150.87	1986	2010	TV	
ROSSLYN BAY	Rosslyn Bay	1760	RLR	Yes	−23.16	150.79	1994	2010	TV	
HAY POINT	Hay Point	1246	RLR		−21.28	149.30	1985	2010	TV	
MACKAY	Mackay	564	RLR		−21.10	149.23	1966	2010	TV	
SHUTE HARBOUR 2	Shute Harbour	1569	RLR		−20.28	148.78	1983	2010	TV	
BOWEN II	Bowen	2074	RLR		−20.02	148.25	1987	2010	TV	
CAPE FERGUSON	Cape Ferguson	1492	RLR	Yes	−19.28	147.06	1992	2010	TV	
TOWNSVILLE I	Townsville	637	RLR		−19.25	146.83	1959	2010	TV	
LUCINDA	Lucinda	1630	RLR		−18.52	146.38	1986	2010	TV	
MOURILYAN HARBOUR	Mourilyan Harbour	1629	RLR		−17.58	146.08	1985	2009	TV	
CAIRNS	Cairns	953	RLR		−16.92	145.78	1966	2009	TV	
PORT DOUGLAS 2	Port Douglas	1471	RLR		−16.48	145.47	1988	2009	X	Insufficient data
GOODS ISLAND	Goods Island	1368	RLR		−10.56	142.15	1990	2010	TV	
INCE POINT	Ince Point	1300	Metric		−10.51	142.31	1975	2009	TV	
TURTLE HEAD	Turtle Head	1749	Metric		−10.52	142.21	1991	2009	X	Insufficient data
WEIPA	Weipa	1157	RLR		−12.67	141.87	1966	2010	TV	
KARUMBA	Karumba	835	RLR		−17.50	140.83	1985	2010	TV	

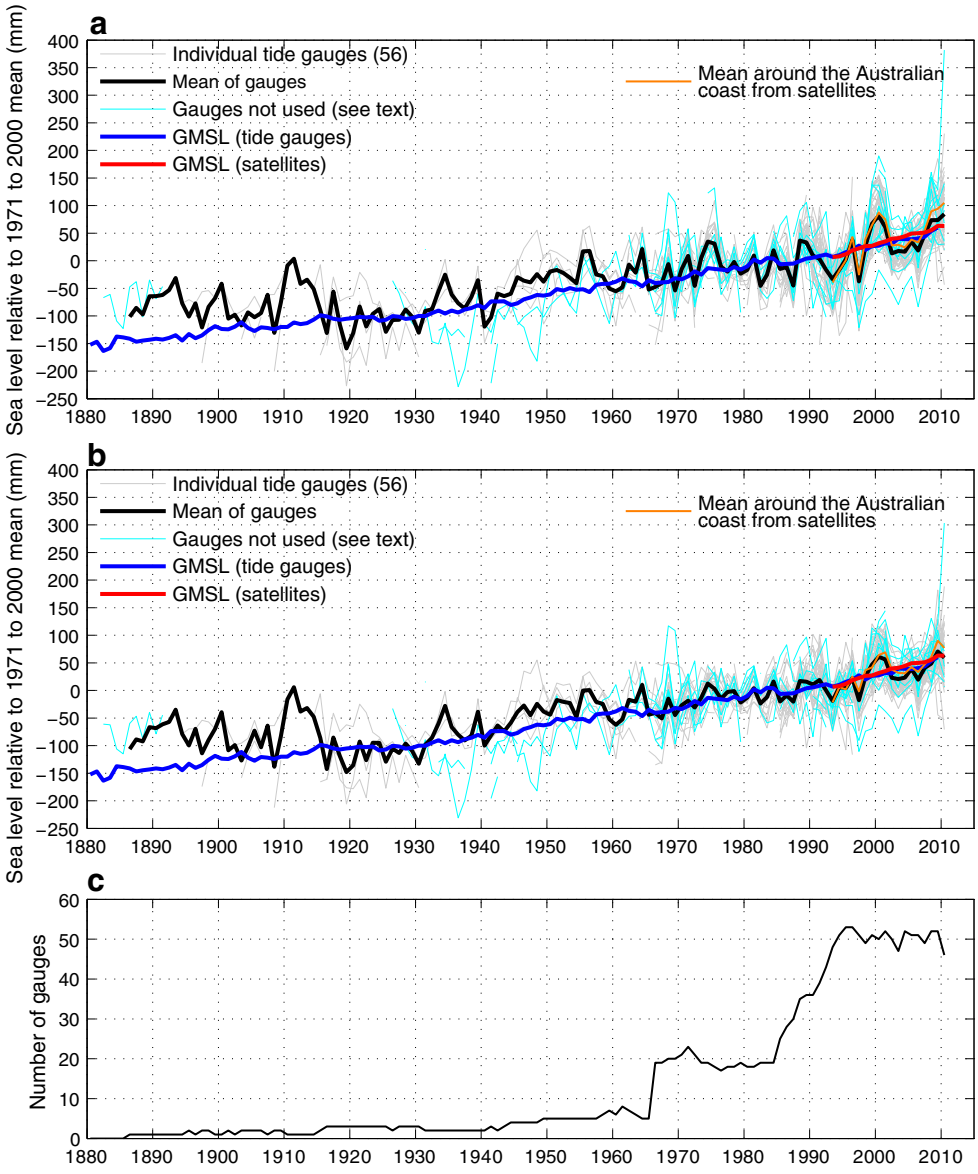

Fig. 2. (a) Overview of Australian sea-level data and comparison with global sea-level estimates, all expressed as OVMSL (Section 2.3). The gauges flagged "TV" in column 10 of Table 1 are plotted in grey. The records flagged because of possible ground movement and credibility issues are plotted in cyan, but not used in calculating averages. The arithmetic mean of the tide gauges considered to be of reasonable quality is plotted as a heavy black line. The GMSL estimated from satellite altimeters (see Section 2.2) is plotted as a heavy red line, and the area-weighted mean from satellite altimeters along a line around the Australian coast is plotted in orange. The cyan trace that goes very high at the end is Wyndham, and the one that goes very low in the 2000s is Point Lonsdale. (b) As in (a) but after the signal correlated with the Southern Oscillation Index is removed (see Section 3). (c) The changing number of gauge stations available for use over time.

to an Earth-fixed reference frame with its coordinate origin at the time-averaged centre of mass of the Earth (the geocentre). Observations of both relative and geocentric MSL inevitably include some component of GIA, hence we choose to use the term OVMSL to denote any measurement (relative or geocentric) that has been corrected to remove the effects of GIA, and thus imply sea-level change in the sense of changing ocean volume. We do not consider sources of VLM other than GIA for this analysis because of the lack of information available.

While traditional surveying techniques are used to monitor the local stability of a tide gauge relative to the local benchmark, observations from continuously operating Global Positioning System (GPS) sites are the preferred data for computing VLM in the same reference frame as satellite altimetry known as the International Terrestrial Reference Frame (e.g. ITRF08, Altamimi et al., 2011). These geocentric estimates of VLM derived from GPS receivers located at or near to tide gauges enable the transformation from relative to geocentric MSL, and thus allow direct comparison with altimetry (e.g. Wöppelmann et al., 2009; King et al., 2012). Here we use the analysis of sparsely located GPS data from Burgette et al. (2013) that provides VLM at 12 Australian GPS stations (each with at least five years of near continuous GPS data) located within 100 km of tide-gauge locations (Fig. 1; Table 2). These data are processed using the preferred strategy of Tregoning and Watson (2009), including the latest developments in algorithms, particularly relating to the treatment of the atmospheric delay and crustal loading induced by the atmosphere. We estimate VLM from the GPS coordinate time series using a maximum likelihood approach as implemented in the CATS (Create and Analyse Time Series) software (Williams, 2008). Further detail on the approach and noise models (consistent with other studies that investigate noise properties across the global tracking network, e.g. Santamaría-Gómez et al., 2011) can be found in Burgette et al. (2013).

The GPS-derived VLM estimates (Table 2) suggest subtle subsidence at many sites, however velocities at 7 of the 12 sites are not significantly different from zero at the one standard error (typically 0.3 to 0.8 mm yr^{-1})

Table 2
Vertical land motion (VLM) at the 12 GPS sites located within 100 km of tide gauges and having at least 5 years of continuous GPS data. VLM estimates provided include linear rates derived from GPS (GPS VLM, mm yr^{-1} ± 1 standard error), the predicted GIA crustal velocities (GIA VLM, mm yr^{-1}) and the GIA induced contribution to relative mean sea level (GIA RMSL, mm yr^{-1}). GPS VLM estimates (from the CATS analysis), significantly different from zero at the one standard error level are shown in italics. GPS and GIA VLM velocities are in the sense of positive being up. For the GIA RMSL trends, a negative number means that the land is rising with respect to the sea surface.

Site no.	Latitude	Longitude	Data start	Data end	n	GPS VLM	GIA VLM	GIA RMSL
HOB2	−42.8047	147.4387	2000.1	2011.0	24,178	0.0 ± 0.5	−0.2	−0.2
BUR1	−41.0501	145.9149	2002.2	2007.0	10,766	−0.2 ± 0.8	−0.1	−0.2
TOW2	−19.2693	147.0557	2000.1	2011.0	24,164	−0.2 ± 0.4	−0.0	−0.2
DARW	−12.8437	131.1327	2000.1	2011.0	22,414	*−1.6 ± 1.4*	0.0	−0.3
KARR	−20.9814	117.0972	2000.1	2011.0	24,262	0.2 ± 0.8	−0.1	−0.2
HIL1	−31.8255	115.7386	2003.0	2011.0	17,654	*−3.1 ± 0.7*	−0.1	−0.2
PERT	−31.8019	115.8852	2000.1	2011.0	22,939	*−2.1 ± 0.7*	−0.1	−0.2
YAR2	−29.0466	115.3470	2000.1	2011.0	24,626	*0.9 ± 0.4*	−0.1	−0.2
MOBS	−37.8294	144.9753	2002.8	2011.0	18,865	−0.3 ± 0.5	0.0	−0.3
CEDU	−31.8667	133.8098	2000.1	2011.0	24,213	−0.3 ± 0.4	−0.1	−0.3
SYDN	−33.7809	151.1504	2005.4	2011.0	12,803	−0.4 ± 0.7	−0.1	−0.2
ADE1	−34.7290	138.6473	2000.1	2010.7	23,415	*−0.4 ± 0.3*	−0.0	−0.3

level. Hillarys (HIL1) and Perth (PERT) show land subsidence that is likely associated with fluid extraction (Deng et al., 2011; Featherstone et al., 2012) with, possibly, an extra contribution from land settlement at Hillarys, highlighting that localised effects are important in some regions. The Adelaide GPS (ADE1) site also shows subsidence, but at a slower rate than for Hillarys, consistent with earlier analysis (Belperio, 1993). The Darwin site (DARW) shows subsidence, but at a rate that is only just significant at the one standard error level. We note that the Darwin site has the largest formal uncertainty, highlighting that the linear plus periodic components model used to describe the time series are a poor descriptor of the complex quasi-seasonal energy, largely of hydrological origin, that is evident in the time series for Darwin (e.g. Tregoning et al., 2009). The Yarragadee GPS site (YAR2, which is ~45 km inland) has a significant positive (upward) vertical motion, and, with the exception of a possible effect from an uncalibrated antenna radome and a time variable GPS constellation, we have no explanation for the trend observed at this site.

The predicted contribution of GIA to VLM may be compared with the GPS based estimates of VLM (Table 2). Using the model described in Tamisiea (2011), we extract both the contributions of GIA to VLM (hereon GIA VLM), as well as its contribution to relative MSL (hereon GIA RMSL), at sites around Australia where VLM is directly measured using GPS data. The GIA-induced crustal motions throughout the 20th century are small, but mostly negative ranging from −0.2 mm yr^{-1} to 0.0 mm yr^{-1} at these locations. The corresponding contributions to RMSL change at these sites are all negative (Table 2), but again small. At the 69 tide gauge sites used in this study, GIA alone would cause a RMSL fall by −0.1 to −0.4 mm yr^{-1} (Tamisiea, 2011; Fleming et al., 2012). That is, for the 20th and 21st centuries, these GIA motions cause RMSL rise around Australia to be lower than they would otherwise be.

In summary, predictions of GIA and measurements from GPS show that vertical land movements around most of the Australian coastline are small, with more pronounced localised subsidence at a few specific sites.

2.4. Climate indices

In order to investigate the inter-annual variability of MSL and how it might be affected by regional climate variability, we make use of six climate indices. The Southern Oscillation Index (SOI) is a descriptor of the El Niño-Southern Oscillation (ENSO) (Walker, 1923; Montgomery, 1940). Sustained negative values of the SOI indicate El Niño episodes and positive values are associated with La Niña events. The Multivariate ENSO Index (MEI) is a more complete and flexible descriptor of ENSO (Wolter, 1987; note that its definition has the opposite sign to the SOI). The Pacific Decadal Oscillation (PDO) is a pattern of climate variability with a similar expression to El Niño, but acting on a longer time scale, and with a pattern most clearly expressed in the North Pacific/North American sector (Trenberth and Hurrell, 1994). The Interdecadal Pacific Oscillation (IPO) (Power et al., 1999; Parker et al., 2007) is a manifestation of the PDO covering more of the Pacific Ocean (down to 55°S). The Indian Ocean Dipole (IOD), represented by the Dipole Mode Index (DMI), is a coupled ocean–atmosphere phenomenon in the Indian Ocean and has a strong relationship to ENSO (Saji et al., 1999). The Southern Annular Mode (SAM) effectively indicates the strength of the westerly winds in the Southern Oceans (Gong and Wang, 1999). The source of the different climate indices uses in this paper, periods covered and a brief description of how they are calculated are listed in Table 3.

3. Australia-wide sea-level variability and trends

We focus here on the 45 year period from 1966 to 2010 (inclusive) as this is the longest period for which data is available around the whole country. There are 16 near-continuous tide-gauge records

Table 3
Definitions and sources of climate indices.

Climate Index	Period	Description
SOI	1880–2011	Defined as the normalised air pressure difference between Tahiti and Darwin. http://www.bom.gov.au/climate/current/soihtm1.shtml
MEI	1950–2011	Based on six observed variables over the tropical Pacific, namely: sea-level pressure, zonal and meridional components of the surface wind, sea surface temperature, surface air temperature, and total cloudiness fraction of the sky. http://www.esrl.noaa.gov/psd/enso/mei/mei.html#data
PDO	1900–2011	Defined as the leading principal component of North Pacific SST variability. http://jisao.washington.edu/pdo/
IPO	1880–2008	Defined as the leading principal component of North and South Pacific SST variability. http://www.iges.org/c20c/
DMI	1880–1997	The intensity of the IOD is represented by the SST anomaly difference between the eastern and the western tropical Indian Ocean. This gradient is named the Dipole Mode Index (DMI). http://www.jamstec.go.jp/frsgc/research/d1/iod/e/index.html
SAM	1948–2011	Defined as the normalised air pressure difference between 40°S and 70°S. http://web.lasg.ac.cn/staff/ljp/data-nam-sam-nao/sam-aao.htm

providing coverage of all areas of the Australian coastline with the exception of the Gulf of Carpentaria (Figs. 1, 3). Coverage is significantly lower before 1966 (Fig. 2c). After 1993, there are more than twice the number of records available but the spatial coverage is similar, with the exception of an additional gauge in the Gulf of Carpentaria.

3.1. Variability

Seasonal (annual and semi-annual) signals were removed from each record by estimating simultaneously annual and semi-annual sinusoids using least squares. After filling 1-month gaps by spline interpolation we filled the remaining small gaps (max length 58 months) in records at 10 stations with data from the neighbouring stations. In all, 298 months were filled (3.4% of the total). This procedure is justified by the clear along-shore coherence between nearby gauges and the fact that leaving out the record with the largest gap makes minimal difference to the results. The variances of the monthly MSL are a maximum at Darwin in the north and decrease going anti-clockwise around Australia (with a second maximum in the South Australian gulfs) to Townsville, for which the variance is less than half that at Darwin (Table 4, col. 3). Note that we use records from Port Adelaide (Outer) and Newcastle here to focus on variability rather than trends but trends from these records are not used, due to datum and subsidence issues as discussed previously. We calculated a low-frequency component using a one-year low-pass filter, using a Finite Impulse Response (FIR) filter (−6 dB at one year)—see Fig. 4, solid lines. Empirical Orthogonal Functions (EOFs; Preisendorfer, 1988) were calculated from the low-passed, de-trended (using least squares) data to identify the variability that is common to many records and the Principal Component (PC) time series were correlated against each of the six regional climate indices.

For the high frequency component (the difference between the original monthly time series and the low-passed time series), the variances are largest on the south coast where the strong westerly winds and the wide shelf generate large amplitude coastal-trapped waves (Provis and Radok, 1979; Church and Freeland, 1987). The first EOF mode of the high frequency component (not shown), accounting for almost 50% of the variance, has maximum amplitude on the south coast, decreasing northwards along the east coast, and little signal on the west coast.

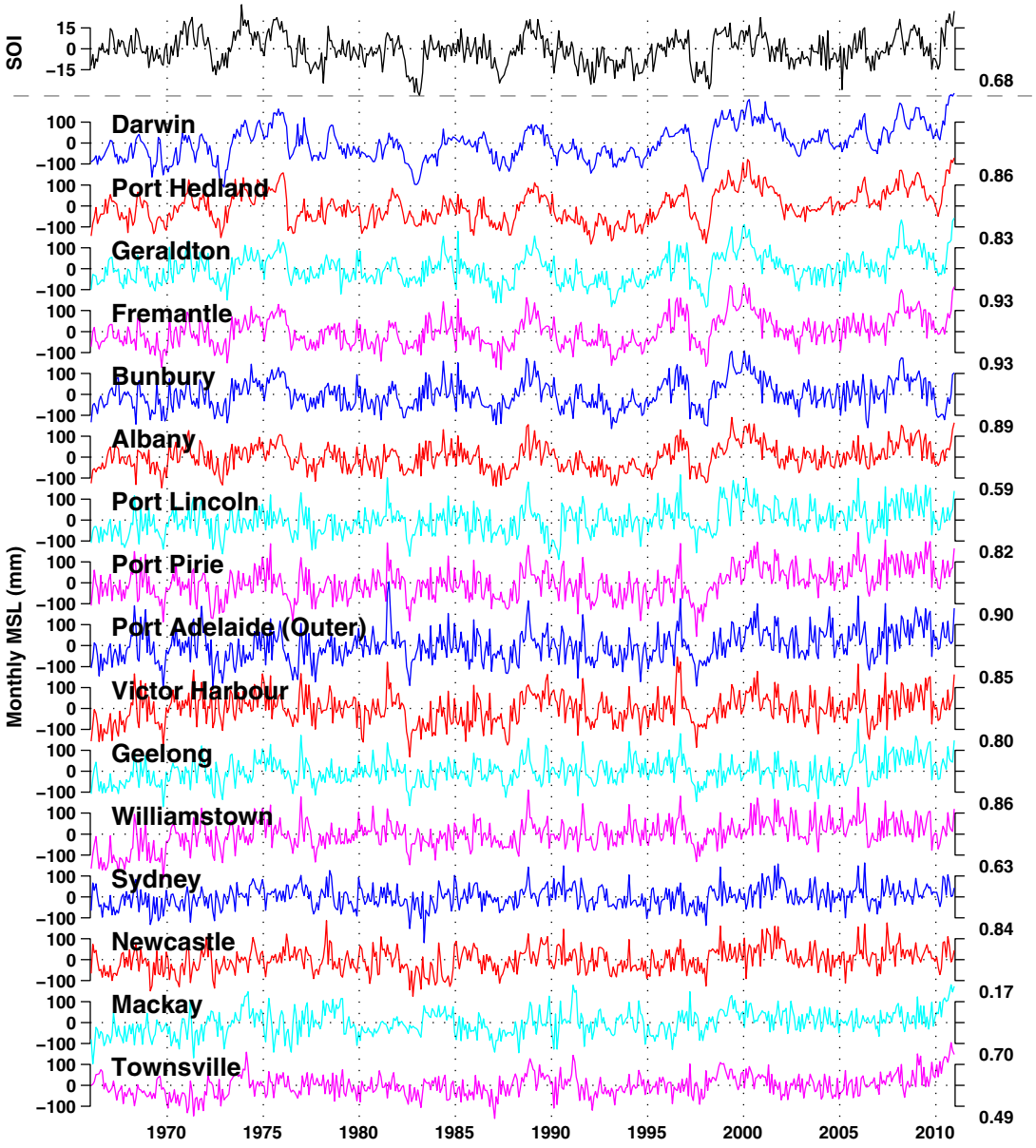

Fig. 3. Monthly RMSL time series for the 16 near continuous records available for January to December 2010, from Darwin in the north, anticlockwise to Townsville in the northeast. The SOI is also shown. Cross-correlations between adjacent time series are shown on the right. The cross-correlation between Townville and Darwin is shown below Townsville.

Table 4
RMSL and OVMSL linear trends (mm yr^{-1}) and variances (mm^2) of sea-level records for the period 1966 to 2010. A low-pass filter (see text) is used to obtain the low- and high-frequency components. The variances of the unfiltered and filtered monthly data (columns 3 and 5) are calculated after removal of a linear trend (columns 2 and 4). The variances after removing the component of the first EOF linearly correlated to ENSO and the linear trend are given in columns 7 and 6. The linear trend after removal of the SOI-correlated signal and including the adjustment for atmospheric pressure and GIA is given in column 8. The means and standard deviations in the last row only use data from 14 of the 16 stations—i.e. not including Port Adelaide and Newcastle—see Table 1 and the associated discussion.

1	2	3	4	5	6	7	8
Site	Monthly		+ low-pass filter		+ ENSO removal		+ → OcVol
	RMSL trend (mm yr^{-1})	res var (mm^2)	RMSL trend (mm yr^{-1})	res var (mm^2)	RMSL trend (mm yr^{-1})	res var (mm^2)	OVMSL trend (mm yr^{-1})
Darwin	2.6	5429	2.4	4129	2.7	999	3.1
Port Hedland	1.8	5351	1.5	3920	1.9	1126	2.1
Geraldton	1.2	4787	1.0	3064	1.3	1040	1.5
Fremantle	1.8	4615	1.7	2920	2.0	965	2.3
Bunbury	0.9	4524	0.8	2637	1.1	1140	1.4
Albany	0.9	3547	0.8	2039	1.1	757	1.4
Port Lincoln	1.9	4130	1.9	1632	2.0	944	2.3
Port Pirie	2.0	5102	2.0	2349	2.2	1321	2.6
Port Adelaide (Outer)	*1.7*	*5518*	*1.6*	*2161*	*1.9*	*1304*	*2.2*
Victor Harbour	0.8	5306	0.7	2193	0.9	1335	1.2
Geelong	1.2	3269	1.1	1271	1.3	907	1.7
Williamstown	2.1	3689	2.0	1420	2.2	1132	2.7
Sydney	0.8	2497	0.8	819	0.9	620	1.3
Newcastle	*1.2*	*3149*	*1.2*	*1180*	*1.3*	*823*	*1.8*
Mackay	1.5	3099	1.3	1184	1.4	1077	1.8
Townsville	1.3	2474	1.2	980	1.3	751	1.8
Mean (s.d.)	1.5 (0.6)		1.4 (0.5)		1.6 (0.6)		1.9 (0.6)

EOF 2, accounting for almost 20% of the variance has a maximum on the west coast and EOF 3 has a maximum amplitude on the east coast. These results are consistent with wind forced coastal-trapped waves propagating south along the west coast (Hamon, 1966), east across the Great Australian Bight (Provis and Radok, 1979; Church and Freeland, 1987) and northwards along the east coast (Hamon, 1966; Church et al., 1986a,b; Freeland et al., 1986).

Low frequency variability (i.e. inter-annual or longer) dominates the MSL time series at Darwin (over 4000 mm^2, 75% of the total variance at Darwin) and the monthly anomalies appear to propagate rapidly southward along the west coast of Australia, eastward along the south coast (the direction of coastal-trapped wave propagation), but with the magnitude of perturbations decreasing with distance (Fig. 4, Table 4, col. 5). The perturbations are almost in phase along the east coast and have a smaller variance (of order 1000 mm^2; about 30% of the total at each location) than on the west and south coasts. The first EOF mode of the low-passed signals (Fig. 5a), accounting for 69% of the variance, has a simple spatial structure of decreasing amplitude around Australia. Correlations and lags between Principal Component 1 (PC 1), i.e. the time series associated with the first EOF, Fig. 5b are most highly correlated with the SOI (+0.87 at 0 lag). Maximum correlations and their associated lags for the six climate indices are shown in Table 5. EOF 2 only explains about 11% of the variance, has maximum amplitude along the south coast and the maximum correlation with climate indices is with the SAM (−0.43 at 0 lag).

The large percentage variance explained by one EOF, its simple spatial structure, and its high correlation with the SOI (and other Pacific climate indices) suggests that it should be possible to robustly remove significant inter-annual and decadal variability from individual records. To do this, for each location i we produce an ENSO-removed time series ($h_{er,i}$) as follows:

$$h_{er,i} = h_{or,i} - e_i \times \lambda_1 \times b \times SOI$$

where: $h_{or,i}$ is the original (low-passed) RMSL time series, as on Fig. 4 at location i, e_i is the value of EOF 1 at location i (as on Fig. 5a), λ_1 is the eigenvalue associated with EOF 1, b is the regression coefficient of PC 1 against the SOI (SOI being the independent variable) and SOI is the low-pass filtered SOI time series.

For Darwin, this simple procedure reduces the variance about the linear best fit by about 75% (Fig. 4, dotted lines; Table 4 col. 7) with the resultant time series having reduced inter-annual to decadal variability. For other locations, variance of the order of 60% was removed on the west coast, 30–50% on the south coast, and 15–30% on the east coast. This process very effectively reduces the differences between the time series (Fig. 6a and b), allowing more accurate estimation of the long-term trends in RMSL, which in turn leads to a clearer picture of the spatial variation in trends.

We also tested more complicated schemes where there was a direct correlation between the SOI and each individual record, including allowing for a time lag, and following Zhang and Church (2012), simultaneously regressing each RMSL record against a high passed version of the SOI and a low passed version of the PDO. Although these models have a greater number of parameters, the results were very similar. As a result, for further analysis, we used the simple scheme that exploited the highly correlated nature of the variability; i.e. using the EOF signal correlated with SOI. This simple model is adequate for this analysis. We also note that, although the low-passed sea level and SOI mainly contain variations at inter-annual time scales, there is still some variability at longer time scales. There is debate on whether the PDO and ENSO are totally independent of each other, since the PDO and ENSO are highly correlated at decadal and longer time scales (Newman et al., 2003; Power and Colman, 2006). The low-passed sea level and SOI contain not only inter-annual variability but also decadal (and longer) variability, which could be associated with ENSO and PDO. See Zhang and Church (2012) for a more detailed discussion of the relationship between ENSO and the PDO.

3.2. Trends

Fourteen of the sixteen gauges are useful for calculating trends (Section 3.1). The 1966–2010 average of the RMSL trends from the monthly data, from these 14 tide gauges is about 1.5 mm yr^{-1}, with a range from 0.8 mm yr^{-1} at Sydney and Victor Harbour to 2.6 mm yr^{-1} at Darwin. The 14 rates have a standard deviation of 0.6 mm yr^{-1} (Table 4). Trends are derived using linear least squares, and serial correlation is accounted for using an autoregressive error structure of order 1 AR(1) model (Chandler and Scott, 2011). Filtering

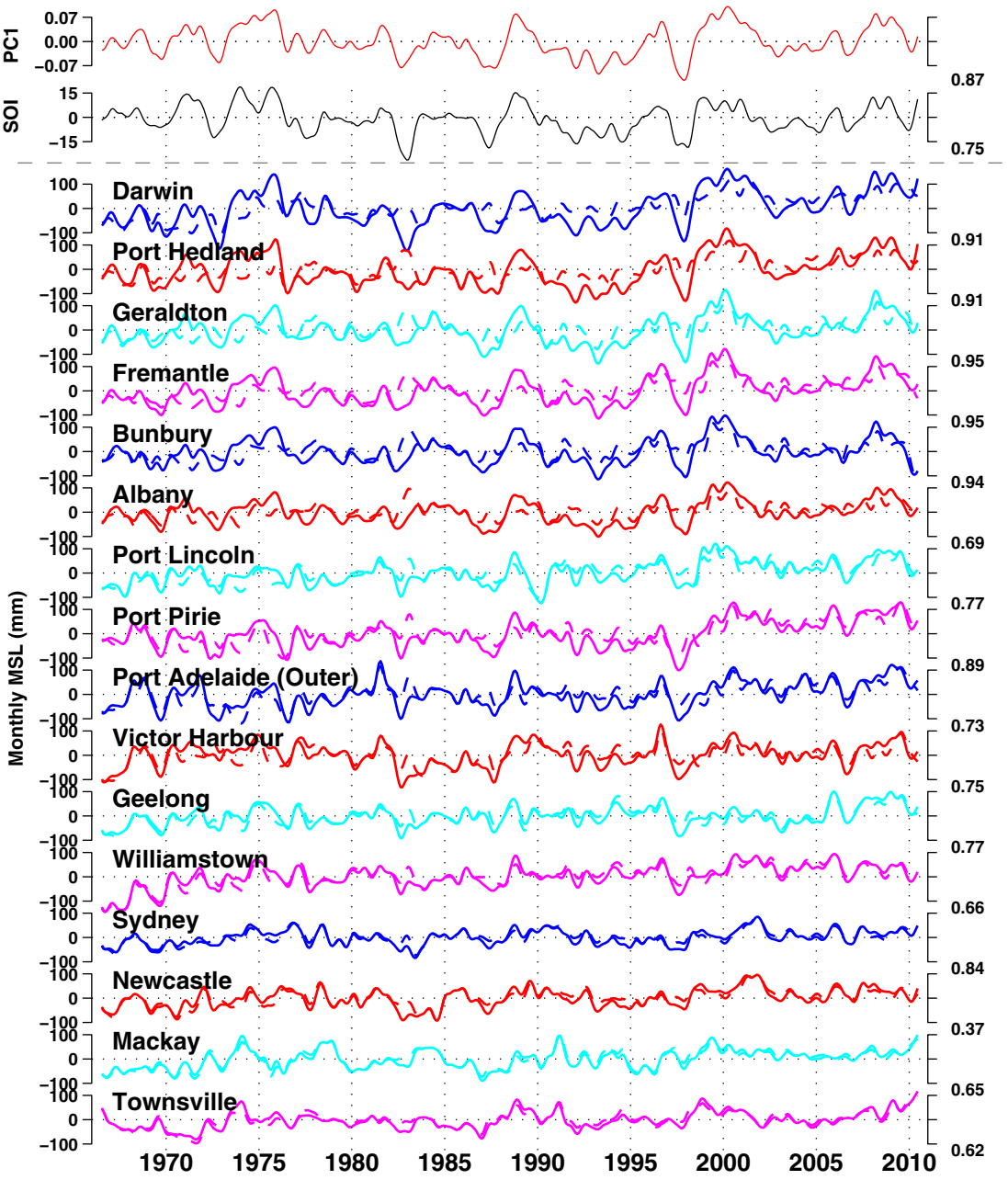

Fig. 4. Low-passed RMSL time series for the 16 near continuous records available for the period 1966 to 2010, from Darwin in the north, anticlockwise to Townsville in the northeast. The low-passed Southern Oscillation Index and PC 1 are also shown. The sea-level records after removing the inter-annual variability represented in the first EOF and linearly related to the SOI are shown by the dashed lines. Cross-correlations are shown as for Fig. 3.

and calculation of anomalies is as in Section 3.1. There is clearly significant inter-annual variability about the long-term trends in each of the records (Figs. 3 and 6a) that is directly related to inter-annual climate variability. Much of this inter-annual variability can be removed using the strong zero lag correlation of PC 1 with the low passed SOI (Fig. 6b, Table 4) thus reducing the residual from a line of best fit by up to about 80% at some locations. Clearly some inter-annual variability remains that is not directly correlated with ENSO.

The trends (± 1 standard error) of the mean of the 14 records after low-passing and removal of the ENSO-correlated signal (as in columns 6 and 7 of Table 4) are 1.6 ± 0.2 mm yr^{-1} for 1966 to 2010, 2.2 ± 0.5 mm yr^{-1} for 1990 to 2010 and 2.4 ± 0.6 mm yr^{-1} for 1993 to 2010. For comparison with global MSL trends we use the Church and White (2011) time series. This time series ends in 2009, and is in the sense of OVMSL (Section 2.3), so we convert the tide gauge RMSL trends to the sense of ocean volume and calculate trends ending in 2009 for consistency. For the tide-gauge time series, the OVMSL trends become 1.9 ± 0.2 mm yr^{-1} for 1966–2009, 2.6 ± 0.5 mm yr^{-1} for 1990–2009 and 2.9 ± 0.6 mm yr^{-1} for 1993–2009. The equivalent trends, for the same periods from the global MSL time series are 2.0 ± 0.3, 2.5 ± 0.6 and 2.8 ± 0.7 mm yr^{-1}, indicating that there is good agreement between Australian and global-mean trends, even over short periods, once the ENSO-related variability has been removed and the correction for GIA made.

Further smoothing of these records (with a ten year running mean) reveals a period of rising (with some variability) RMSL (Fig. 6c and d). The average of these records is shown by the dashed black line in Fig. 6c (expressed in the sense of OVMSL).

There is a distinct pattern of increasing atmospheric pressures over Australia during this period as shown by the linear trends from the

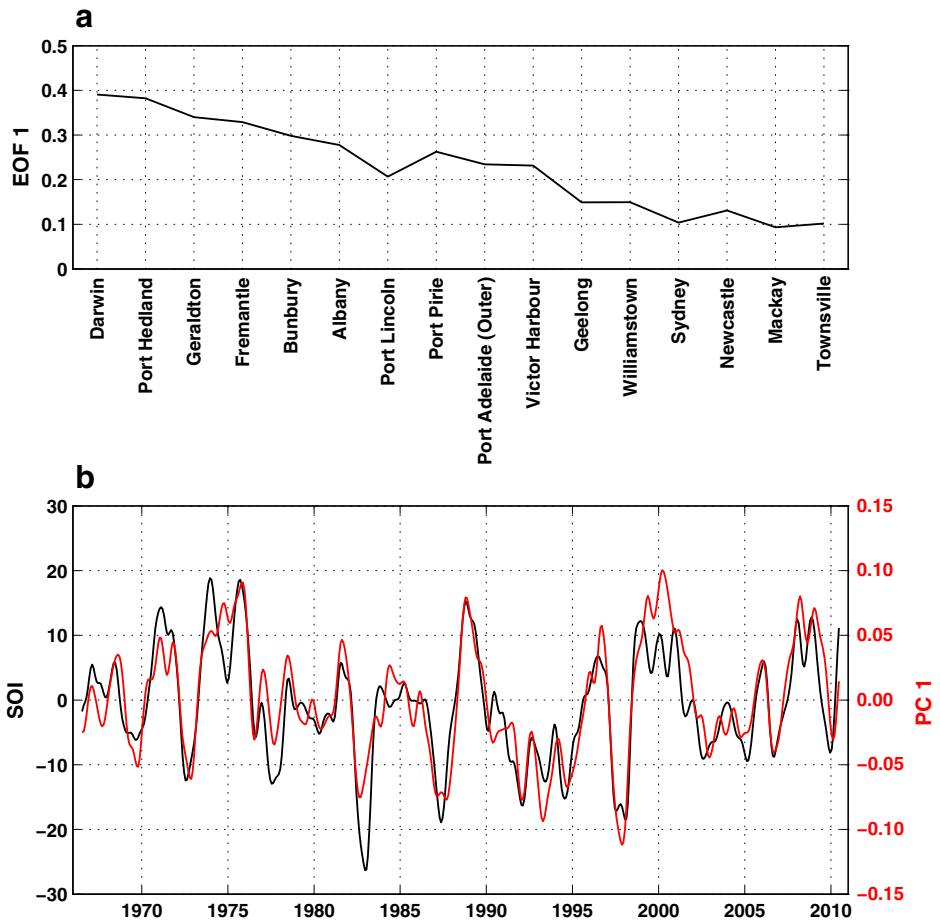

Fig. 5. (a) The first EOF of the low passed sea-level time series plotted against the tide-gauge sites; and (b) the corresponding PC and low-passed SOI plotted against time.

HadSLP2 data set (Allan and Ansell, 2006), slightly depressing observed sea level trends, particularly in the east and north-east of Australia (Fig. 7). This depression of sea level is about 0.2 mm yr^{-1} for the majority of the east Australian coast and over 0.25 mm yr^{-1} from 28°S to 36°S. If we then also apply the inverse barometer correction the mean Australian tide gauge trends become 2.1 ± 0.2, 2.9 ± 0.5 and 3.1 ± 0.6 mm yr^{-1} for 1966 to 2009, 1990 to 2009 and for 1993 to 2009, respectively, still close to the global-mean rates (Table 6).

4. Trends over other periods

We now examine the trends of RMSL (for records that are at least 80% complete as indicated in Table 1) as measured directly by the tide gauges (i.e. without any corrections for VLM or the inverse barometer effect). We focus here on two periods: the first being that spanned by the two longest tide gauge records (Sydney from 1886 to 2010 and Fremantle from 1897 to 2010); and the second being the period from January 1993 to December 2010 when many more tide gauge records (57), and also satellite altimeter data, are available. Different but related statistical approaches have been used to analyse data from these three periods; the chosen methodology depends upon whether the focus is on specific or multiple gauge sites, the length of series, and how best to quantify and remove inter-annual variation. Uncertainties in trends are expressed as one standard error (i.e. 68% confidence level).

Table 5
Maximum correlations and their associated lags between PC 1 and the climate indices. A positive lag indicates that the index is later than PC 1.

Index	Correlation	Lag (months)
SOI	+0.87	+0
MEI	−0.84	+1
PDO	−0.63	+3
IPO	−0.82	+1
SAM	+0.26	−9
DMI	−0.43	+0

4.1. The long records

Monthly RMSL data from Australia's two longest recording sites (Fremantle and Sydney) were independently used to search for the presence of both linear and non-linear long-term trends (Fig. 8a and b respectively). An extended multiple regression method known as generalised additive models (GAMs; Wood, 2006) was used as the basis for developing a flexible statistical model to quantify non-linear smooth time trends in RMSL. GAMs have an advantage over the more globally-fitting models such as polynomials in that nonlinearity is fitted locally and hence trends can be of an arbitrary shape. The process implemented closely followed that of Morton and Henderson (2008).

A general statistical model was proposed, the components of which accounted for: (i) seasonality (annual and semi-annual variability); (ii) a climate 'noise' covariate (inter-annual variability as measured by SOI since the EOF technique cannot be applied to a single RMSL series); (iii) nonlinear trend (modelled as a spline, see further details below); and (iv) serial correlation (autocorrelation) of the residual terms. The model took the form:

$$\begin{aligned} RMSL_i = {} & \alpha_1 \cos(2\pi t_i - \varphi_1) + \alpha_2 \cos(4\pi t_i - \varphi_2) && \text{seasonality} \\ & + \beta\ SOI && \text{climate} \\ & + \gamma_1 + \gamma_2 t_i + s(t_i; df) && \text{time trend} \\ & + \varepsilon_i && \text{noise} \end{aligned} \quad (1)$$

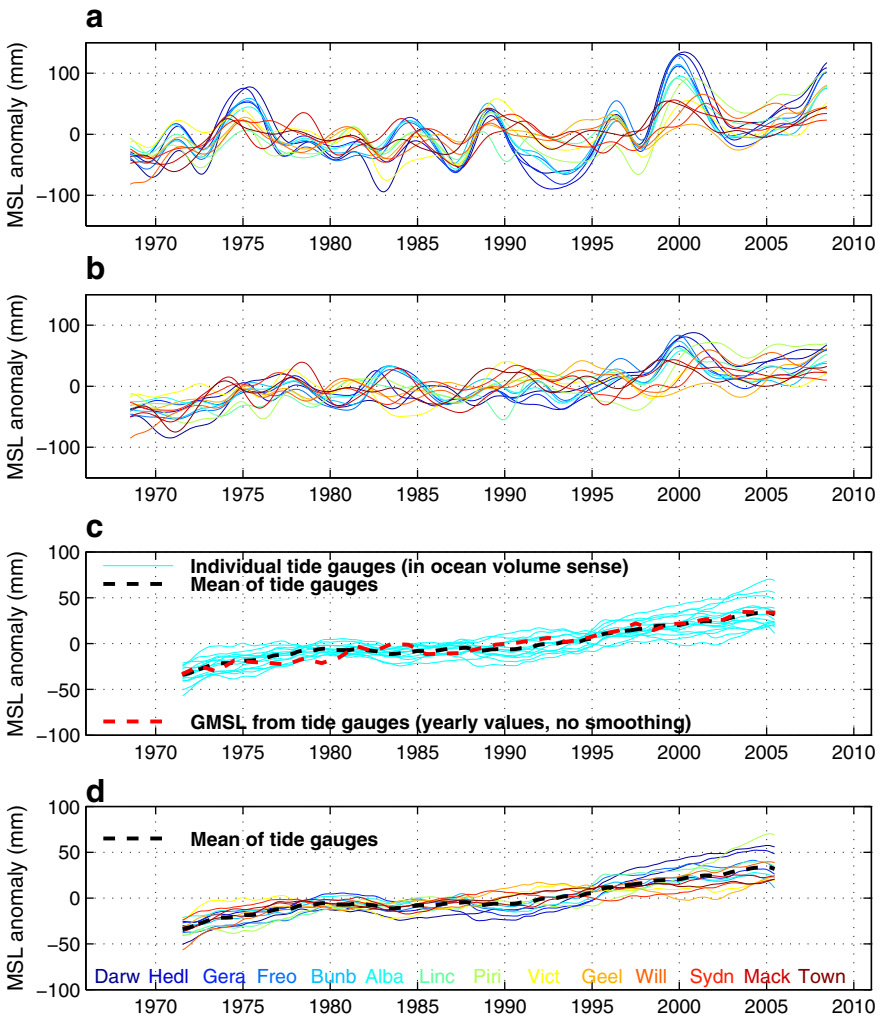

Fig. 6. (a) Low-passed RMSL sea levels for the 14 records available for 1966 to 2010, and (b) after the component of EOF 1 related to ENSO have been removed. Note: Newcastle and Port Adelaide (Outer) are not displayed. In (c), the data smoothed with a ten year running average are compared with the average of the records and the global mean sea level from Church and White (2011). (d) As in (c), but with the 14 tide-gauge records plotted in different colours to more easily distinguish them. Data displayed on panels (c) and (d) is in the sense of OVSML.

where i refers to successive monthly observations and t_i = time in years. The amplitude and phase of the annual and semi-annual seasonal periodic terms (α_1, φ_1 and α_2, φ_2, respectively) were estimated from the linear coefficients of orthogonal sine and cosine basis functions in each case. Inter-annual variability was modelled as a linear relationship between SOI and RMSL (regression coefficient β), with SOI being filtered using a 3 month running mean to mimic its short term cumulative effect upon RMSL. The time trend was composed of two parts: the first being the linear component $\{\gamma_1 + \gamma_2 t_i\}$ where γ_1 is the model's intercept term and γ_2 is the estimated linear rate of change spanning the full time series; and the second denoted by $s(t_i; df)$, is a cubic smoothing spline with formal degrees of freedom df chosen as 6 for this analysis. This spline term accounts for deviations from linearity over time, with a flexibility approximately equivalent to a polynomial of a similar degree (df) (Morton and Henderson, 2008). An autoregressive error structure of order 1 (AR(1)) was included in the model whereby the error for ith observation is formed as $\varepsilon_i = \rho\varepsilon_{i-1} + \xi_i$, with ρ being the estimated first order autocorrelation and ξ_i is an independent random error term. All parameters were estimated using the method of maximum likelihood. The model was implemented using the statistical software package R (The Comprehensive R Network: http://cran.r-project.org/).

Having checked model assumptions via residual diagnostic plots, the model fitted the Fremantle data somewhat better (approximate adjusted $R^2 = 0.67$) than the Sydney data ($R^2 = 0.42$), with all model terms highly significant at both sites. Results from the model fit show significant annual (36.0 and 102.7 mm) and semi-annual (21.2 and 30.4 mm) amplitudes for Sydney and Fremantle respectively (Table 7). Annual maxima in RMSL occur in late May at Sydney, and early June in Fremantle, consistent with other studies (e.g. Fig. 4 in Burgette et al., 2013). Further investigation of the seasonal amplitudes using an alternate technique (not shown here) that treats the model terms as time variable quantities with defined process noise within a Kalman filter (Davis et al., 2012), suggests a possible trend in the annual amplitude at Fremantle (~99 mm in ~1920 to ~104 mm in ~2011). These values lie within the formal error of the GAMs time-constant estimate of 102.7 ± 3.3 mm. About a 10% increase in annual amplitude is evident at Fort Denison (~33 mm in ~1925 to ~37 mm in ~2011), again broadly consistent with GAMs time-constant estimate and standard error of 36.0 ± 2.2 mm.

The results for the linear SOI model term are consistent with the analysis of Section 3 and show a significant correlation of SOI with inter-annual variability in RMSL, with correlation stronger at Fremantle ($r = 0.47$, SOI term $\beta = 3.15 \pm 0.28$) than at Sydney ($r = 0.17$, $\beta = 0.92 \pm 0.18$). Using the alternate Kalman filter strategy, we note small increases in the SOI coefficient over time (~3 in 1920 to ~4 in 2011 at Fremantle, and ~0.2 in 1910 to ~1 in 2011 at Fort Denison), consistent

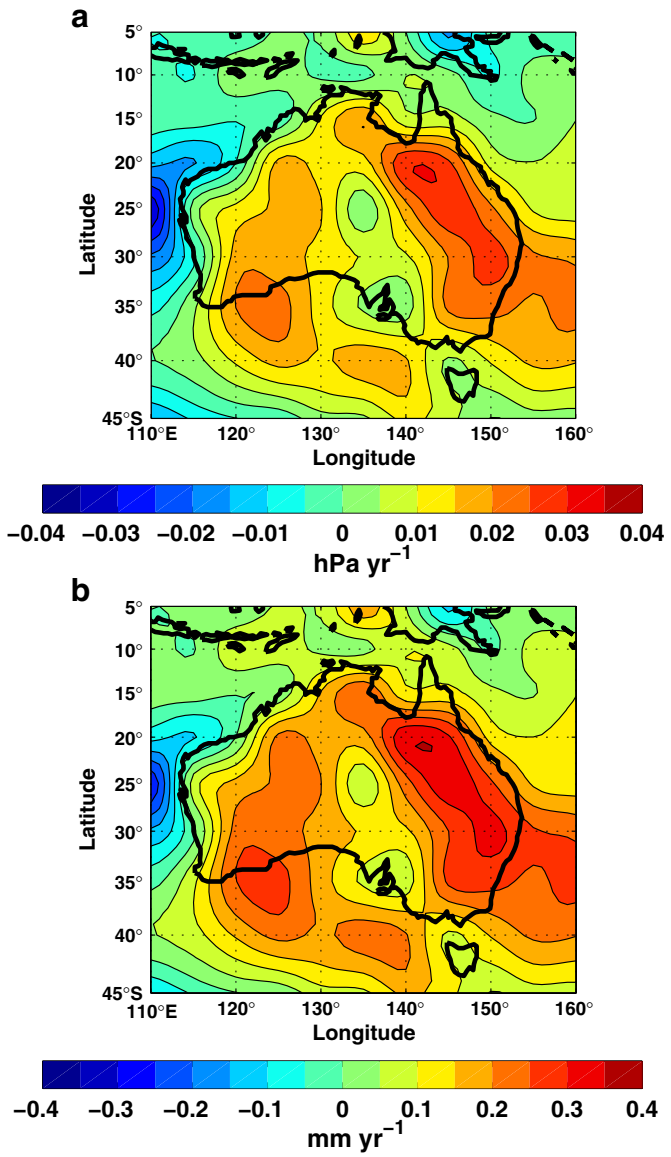

Fig. 7. (a) Trends in local atmospheric pressure from the HadSLP2 data set from 1966 to 2010; (b) equivalent trends in sea level from applying the inverse barometer effect using the atmospheric pressure changes shown on the top panel relative to the time-varying over-ocean global-mean atmospheric pressure.

with the changes observed by Haigh et al. (2011). As per the seasonal terms, this average of the time variable estimates is consistent with the GAMS time invariant model parameters.

The non-linear component of the time trend (i.e. ($s(t_i; df)$, Eq. (1)) is significant at both sites (Table 7). This suggests that the linear component ($\gamma_1 + \gamma_2 t_i$, Eq. (1)) inadequately describes the underlying trend within these data. At Fremantle, the rate of rise (Fig. 8c) is positive over long periods (1897–2010) with an average long-term linear trend of 1.58 ± 0.09 mm yr^{-1} (Table 7). However, between 1920 and 1960 the trend averages to about 2.2 mm yr^{-1}, is near zero from 1960 to 1990, and then increases rapidly to approximately 4.0 mm yr^{-1} over the last two decades. For Sydney (Fig. 8d), RMSL dips curiously between 1910 and 1940, a period which coincides with the digitising of archived charts (Hamon, 1987). RMSL reaches a maximum rate of rise of about 3 mm yr^{-1} around 1950, falls again to a minimum of close to zero in about 1980 and is then rising at 1.5 mm yr^{-1} over the final decades and about 2 mm yr^{-1} at the end of the record. Sydney's rate of rise over all available data (1886 to 2010) is 0.65 ± 0.05 mm yr^{-1} (Table 7) and the 1914–2010 trend is 0.98 ± 0.07 mm yr^{-1}.

In summary, it is clear that RMSL is increasing on average at both sites, and that variability is strongly correlated with ENSO (most significantly at Fremantle). Having accounted for correlation with the SOI and modelling noise using an AR(1) process, the rates of RMSL rise at both sites were found to be non-linear, most significantly for the Fort Denison record. Variation in rates away from the linear trend (Fig. 8c, and d) shows little coherence in time between Fremantle and Fort Denison, suggesting contributions from local effects (e.g. VLM and regional oceanographic and atmospheric variability).

4.2. 1993 to 2010—Comparison of satellite altimeter and tide-gauge data

Results in Sections 3.2, 4.1 and 4.2 suggest that there has been an increase in the rate of MSL rise around Australian since early in the 1990s. The high-quality satellite-altimeter record commences in 1993 following the launch of the TOPEX/Poseidon satellite. Tide-gauge coverage and quality from this time is also significantly improved, with the national ABSLMP array (Bureau of Meteorology, 2011) of high-quality acoustic gauges commencing operation in the early 1990s. Prior to presenting an analysis using all 57 available tide-gauge records covering this period and the off-shore altimeter data, we graphically compare monthly sea-level time series from a subset of representative tide gauges with the altimeter data in Fig. 9. The locations have been chosen to illustrate the range of variability around the coast. In this comparison, we use the unfiltered, monthly tide-gauge data, convert it to the sense of ocean volume, then match the means of the two time series and remove the common mean (the satellite-altimeter data set used here is in the sense of ocean volume). There is no adjustment of the altimeter data to make it agree with tide gauge (or other in situ) data. It is also important to note that this comparison is of sea level observed at the coast (at the tide gauge) with that observed at the nearest offshore altimeter point (~40–200 km away). The altimeter therefore is sampling different oceanic processes that can affect the coherence of two time series (Fig. 9).

The tide-gauge and altimeter time series show a high level of coherence at many sites. At some locations (e.g. Darwin and Milner Bay), the monthly time series are very highly correlated across all time scales, with matching high frequency variability and annual

Table 6
Rates of Australian averaged MSL rise for different periods compared with rates of GMSL. Note OV is ocean volume and AP is atmospheric pressure correction. The first row shows trends without removal of SOI-correlated signals (corresponding to the solid lines on Fig. 4—tagged '(Unc)'). The second, third and fourth rows show trends after removal of the SOI-correlated signals, plus other corrections as noted—tagged '(ER)'. Note also that mean tide-gauge trends shown here are a trend of means, and account is taken of the time varying spread of the tide gauge data. As a result these numbers can be slightly different from the 'mean of trends' numbers shown on the bottom row of Table 4. For example the first number in the third row of this table (1.8) is slightly (but insignificantly) different from it's near-equivalent (1.9) in the last entry in the bottom row of Table 4.

	1966–2010	1990–2010	1993–2010	1966–2009	1990–2009	1993–2009
Tide gauge relative (Unc)	1.4 ± 0.3	4.0 ± 0.9	4.1 ± 1.2	1.4 ± 0.3	4.2 ± 0.9	4.5 ± 1.3
Tide gauge relative (ER)	1.6 ± 0.2	2.2 ± 0.5	2.4 ± 0.6	1.6 ± 0.2	2.4 ± 0.5	2.7 ± 0.6
Tide gauge + OV (ER)	1.8 ± 0.2	2.4 ± 0.5	2.6 ± 0.6	1.9 ± 0.2	2.6 ± 0.5	2.9 ± 0.6
GMSL + OV				2.0 ± 0.3	2.5 ± 0.6	2.8 ± 0.7
Tide gauge + OV + AP (ER)	2.1 ± 0.2	2.6 ± 0.5	2.8 ± 0.6	2.1 ± 0.2	2.9 ± 0.5	3.1 ± 0.6
Altimeter GMSL (OV)			3.3 ± 0.4			3.4 ± 0.4

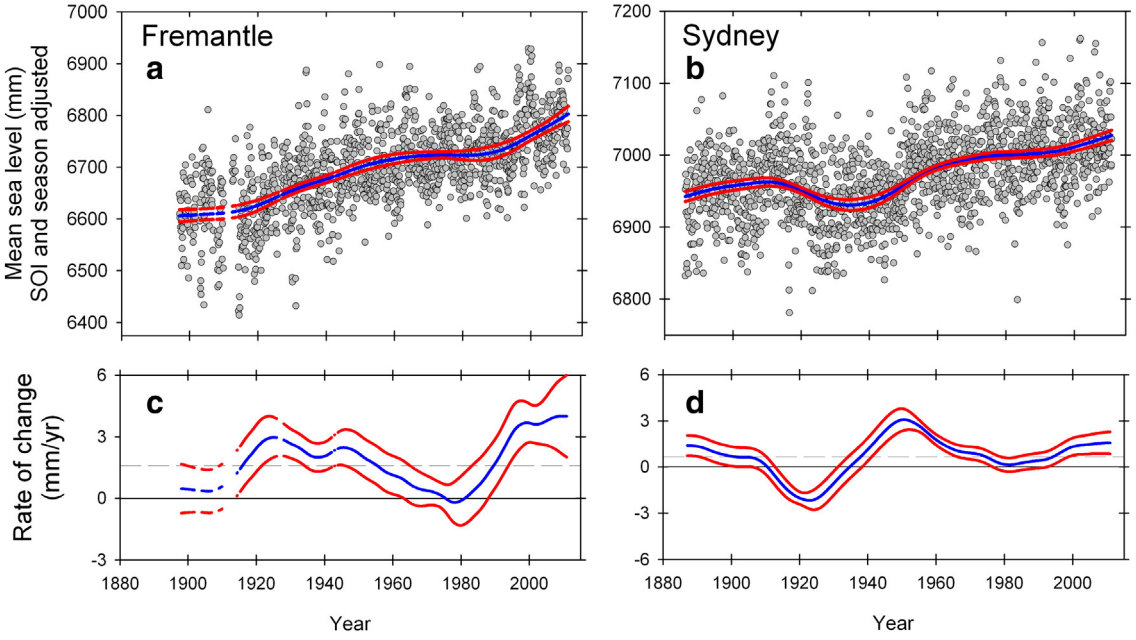

Fig. 8. Upper panels show the fitted generalised additive models (GAMs) and approximate pointwise 95% confidence intervals fitted to RMSL (adjusted for SOI and seasonality) at Fremantle and Sydney. Note the use of different RMSL scales. Lower panels show the non-constant trends as instantaneous rates of change (first differences) and approximate pointwise 95% confidence intervals; dashed lines are the estimated long-term linear trend of 1.58 mm yr^{-1} for Fremantle and 0.65 mm yr^{-1} for Sydney.

signal. At other locations (e.g. Cape Ferguson and Fremantle), the annual signal has a larger variability at the coast than offshore, likely a result of local winds, ocean currents and seasonal temperature and salinity variations on the wide continental shelf. For locations on the southern east coast of Australia, there are significant differences at high frequencies, most likely related to the effect of East Australian Current and its associated mesoscale variability dominating the offshore altimeter record.

A careful comparison for Gold Coast Seaway indicates the section of the tide-gauge record from about 1993 to 1999 is most likely anomalous, probably as a result of a previously undetected datum shift in about 1999/2000. Burgette et al. (2013) verified this finding using differences in adjacent tide gauge time series. More detailed analysis of the altimeter and tide-gauge records at the Burnie site (Fig. 9) confirms the high quality of both records. The Burnie gauge serves as one of few international in situ validation sites for the Jason-class altimeter missions (Watson et al., 2011). When sea levels are estimated off shore from Burnie with in situ instrumentation (such that the altimeter and the in situ observations are both measuring geocentric sea level at the same time), the RMS (Root Mean Square) difference from the two measurements is approximately 30 mm, indicating the quality of the both observing systems and confirming the altimeter systems are observing within their specifications.

Fig. 10a shows linear trends from January 1993 to December 2010 for the Australian region from the satellite-altimeter data (contours), overlaid with estimates from the tide-gauges (coloured dots). Both data sets show the largest trends of up to 12 mm yr^{-1} or more occurring in the north and north west. The lowest trends occur along the east coast of Australia between 20°S and 35°S, with magnitudes generally ranging from about 2 mm yr^{-1} (at about 27°S) to over 5 mm yr^{-1} in the altimeter and tide-gauge data, and off southern Australia where the rates are more than 4 mm yr^{-1}.

In general, the offshore and coastal rates of sea-level change are similar (Fig. 10a), with a few exceptions. As discussed above:

- the Gold Coast seaway contains a datum shift and as a result has anomalously large rates compared to the neighbouring stations and the offshore rates (the red dot on Fig. 10a at about 28°S). The locations where there is significant subsidence, as discussed in Section 2.3 (Hillarys and Port Adelaide), have larger rates in the tide-gauge records than the altimeter series.
- There is a secondary maximum off shore from south-eastern Australia (about 35°S) with peak off shore rates of over 5 mm yr^{-1} but coastal rates of 3–4 mm yr^{-1}. The difference is related to the strengthening of the East Australian Current (Hill et al., 2008; Deng et al., 2011).

Table 7
Estimates of linear parameters (and standard errors) from fitting the long term trend GAM to monthly RMSL data from Fremantle and Sydney. See text for a description of model terms.

			Fremantle		Sydney	
Source	Parameters	Model term	Estimate	S.E.	Estimate	S.E.
Intercept	γ_1	Intercept	3595.88	171.24	5697.95	89.54
Seasonality	α_1	Amplitude	102.68	3.32	35.96	2.20
	φ_1	Phase	2.65	0.03	2.16	0.06
	α_2	Amplitude	30.38	2.51	21.19	1.91
	φ_2	Phase	−0.70	0.08	−1.09	0.09
Climate	β	SOI	3.15	0.28	0.92	0.18
Linear trend	γ_2	t	1.58	0.09	0.65	0.05
Non-linear trend		$s(t_i; df)$	$F_{5,1246} = 3.00$, $P = 0.011$		$F_{5,1487} = 17.64$, $P < 0.001$	
Autocorrelation	ρ	AR(1)	0.45	0.06	0.27	0.05

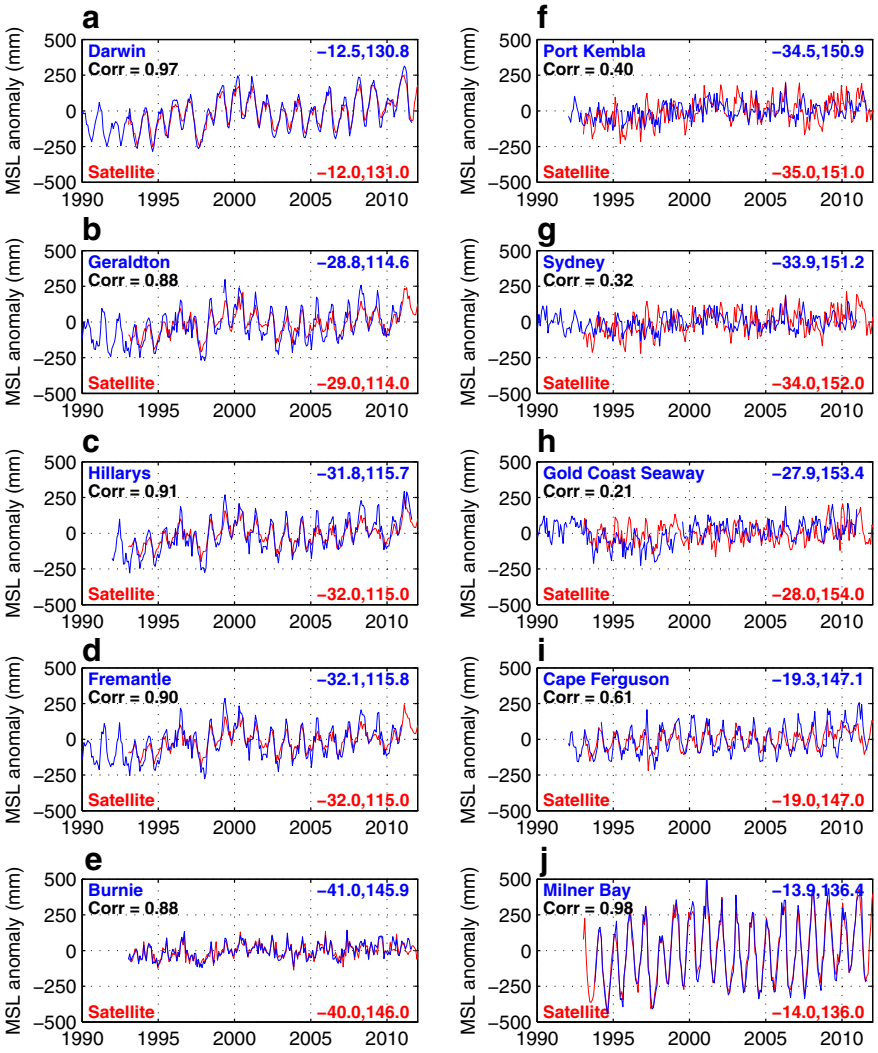

Fig. 9. Comparisons of monthly tide-gauge and satellite-altimeter data, expressed as OVMSL for a selection of locations. Tide-gauge data is plotted in blue, satellite altimeter data in red. Tide gauge names and positions are in blue, and satellite altimeter grid points in red. Correlations between the pairs of time series are shown in black.

- The records at Wyndham and Port Pirie show larger rates of rise but we have no GPS observations to confirm whether this is a result of motion of the tide gauge or more local MSL trends associated with their locations at the head of gulfs and distant from the open ocean.
- Gauges at Eden (south east), Bunbury (south west) and King Bay (north west) all have trends that are anomalous compared with nearby locations to both the north and south. There may be unresolved datum or VLM issues with these records.

As discussed in Section 3 (especially Figs. 3, 4 and 6), there is significant inter-annual variability that is highly correlated with a number of climate indices. Because the 1993 to 2010 period is short, this variability is responsible for a significant fraction of the regional pattern of trends and a linear trend is a poor representation of the longer-term rates of change in MSL, particularly in the north and west of the continent (Zhang and Church, 2012). Fig. 10b shows trends after removal of the ENSO-correlated signal. Note that this is done in a slightly different way to how it is done for 1966–2010, as we don't have EOF values at all locations. A simple regression of the MSL time series against the SOI is used here.

Uncertainties (1 standard error) on the trends shown on Fig. 10 are typically around 1–2 mm yr^{-1}, so there is a clear change in the pattern from this process. Note also that on Fig. 10b most trends around the coast are around 2–4 mm yr^{-1}, consistent with the global mean rate over this period.

5. Discussion

Most assessments of regional RMSL have been in well-instrumented regions of the Northern Hemisphere. The Australian region is perhaps the best instrumented southern hemisphere location for a comparable assessment, as performed here. Australia has the two longest sea-level records in the southern hemisphere, Sydney Fort Denison from 1886 and Fremantle from 1897. The number of tide gauges around the Australian coast increased slowly until the mid 1960s when there was a significant increase to nearly 30. For 1966 to 2010 (45 years, approximately a full PDO cycle and many ENSO cycles) there is almost complete coverage of the Australian coastline. The number of gauges increased further during the late 1980s–early 1990s and we used 57 for this study.

Our analysis indicates considerable inter-annual and decadal variability in RMSL at Australian gauges; largest in the north and west (about 10–15 cm) and smallest in the south and east. A large part of the variability is coherent around the whole of the coastline and is closely related to Pacific Ocean climate variability as represented by (e.g.) the SOI and PDO indices. The RMSL signal is transmitted from the Western

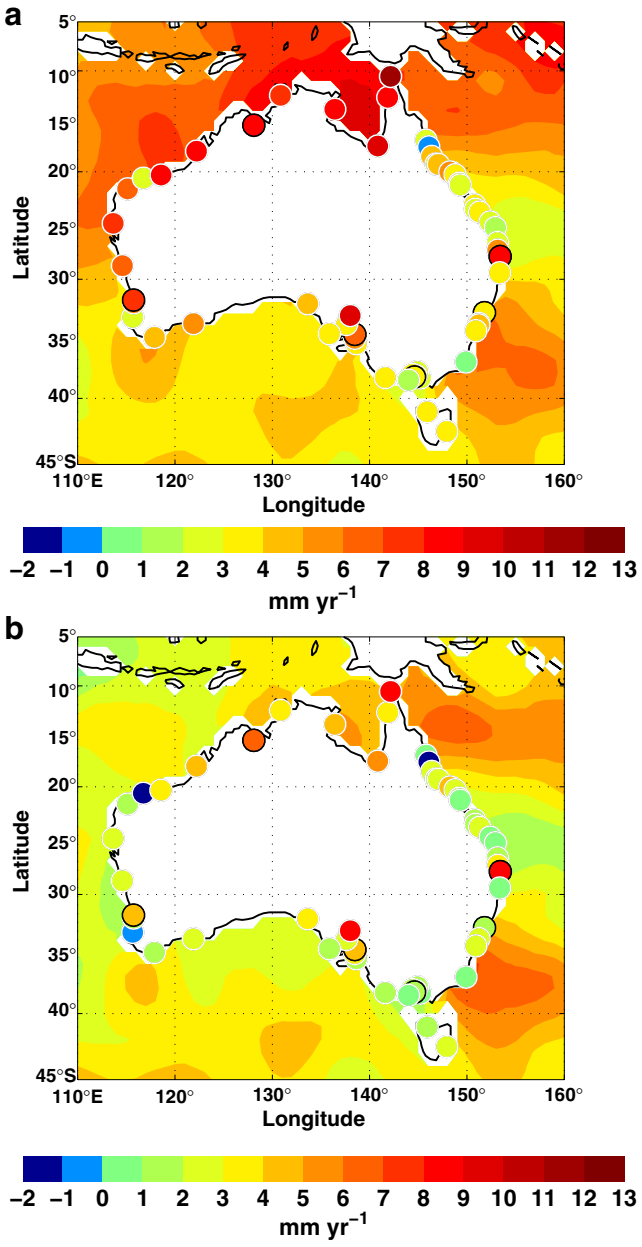

Fig. 10. Sea-level trends from January 1993 to December 2010 from satellite altimeters (colour contours) and tide gauges (coloured dots), both expressed as OVMSL—(a) trends prior to removal of the ENSO signal and b) trends following the removal of the ENSO signal. The red dot on the east coast at 28°S is Gold Coast Seaway—see text. Mean trend differences between altimeter/tide gauge pairs are less than 0.4 and 1.0 mm yr^{-1} (tide gauge mean lower) on panels (a) and (b) respectively. Standard deviations are 2.0 and 2.1 mm yr^{-1} respectively.

Pacific Ocean through the Indonesian Archipelago to Australia's north-west coast (where the variability is highest), from where it propagates anti-clockwise around Australia (Wijffels and Meyers, 2004) with magnitude decreasing with distance. Sea-level variability from the western equatorial Pacific Ocean is weaker along the Australian east coast where westward propagating Rossby wave signals from the subtropical Pacific Ocean directly impact on coastal RMSL (Holbrook et al., 2011). The Indian and Southern Oceans have a much weaker influence on Australian RMSL than the Pacific Ocean.

For 1966 to 2010, a single pattern of inter-annual variability is able to explain 69% of the low-passed variance around the Australian coastline. A simple model based on an EOF analysis of Australian monthly RMSLs and correlation with the SOI removes much of the combined impact of the inter-annual and decadal variability on the observations, reducing the differences in the trends. Our results show that, over decadal and longer periods, geographical differences in the rate of RMSL change around the Australian coastline are related to ocean variability and change rather than to differential land motion (as argued by Aubrey and Emery, 1986).

In comparison to many regions on Earth, much of the Australian coastline is stable in terms of vertical land motion. The GIA component of VLM introduces only small contributions to RMSL (up to about -0.4 mm yr^{-1}, in the sense of the land rising relative to the sea surface). However, localised subsidence at specific tide gauges is important for some sites (e.g. Hillarys, Port Adelaide and, potentially, Darwin), leading to a higher rate of RMSL rise at these locations compared to adjacent tide gauges. These results also highlight the importance of undertaking regional assessments of RMSL, considering data from a number of tide-gauge records, rather than drawing conclusions based on analysis of a single tide-gauge record, even if that record is long. For shorter periods (since 1993) the satellite-altimeter data is a powerful tool.

Changes in atmospheric pressure also influence Australian RMSL by rates up to a few tenths of a millimetre per year over 1966 to 2010. The spatial scale of these changes is again of the order of hundreds to thousands of kilometres with the largest changes being an increase in atmospheric pressure over much of eastern Australia over this period, resulting in a decreased rate of RMSL rise as measured by the tide gauges. This effect can be larger for shorter periods.

The above results indicate that the spatial scale of the variability in RMSL observed in the region is in the order of thousands of kilometres and point to the importance of assessing regional changes. For comparison the New South Wales coastline is approximately 1100 km from end to end. Note, however, that local VLM issues can still be important.

After correcting for the impact of changes in atmospheric pressure (the inverse barometer effect), removing the SOI-correlated signal and expressing estimates in the sense of ocean-volume (i.e. correcting for the effects of GIA), the average Australian trend over 1966 to 2009 was 2.1 ± 0.2 mm yr^{-1} (trend $\pm$ 1 standard error), comparable with the global-average rise over the similar period (1966–2009) of 2.0 ± 0.3 mm yr^{-1}. The GIA contribution is small (~10% of the signal) and will continue essentially unchanged for centuries. The inverted barometer correction is of similar magnitude over recent decades, but can change sign and we would expect the net effect to be small over longer (centennial) time periods. However, these effects are important in understanding Australian sea-level rise and its relationship to global sea level.

Since 1993, Pacific climate variations caused OVMSL on the Australian coastline, particularly in the north and west, to rise much more rapidly than the global mean (as much as four times the global averaged trend) but OVMSL rates of rise were similar to the global average in the southeast of the continent. However, much of this regional pattern is associated with climate variability and, after removal of the SOI-correlated signals, the maximum in the altimeter regional pattern off the northern coasts of Australia is significantly reduced. This pattern is very similar to the results (for 1993 to 2009) of Zhang and Church (2012) who analysed satellite altimeter data and its relationship to the SOI and the PDO.

The two periods (1966 to 2010 and 1993 to 2010) are suggestive of an increase in the rate of rise of Australian (SOI-corrected) OVMSL from 1.8 ± 0.2 mm yr^{-1} to 2.6 ± 0.6 mm yr^{-1}, and 2.1 ± 0.2 mm yr^{-1} to 2.8 ± 0.6 mm yr^{-1} when also corrected for atmospheric pressure effects. The two long records (Sydney and Fremantle) indicate a larger than average rate of rise prior to 1960 (Section 4 and Haigh et al., 2011; Watson, 2011), as does the ocean-volume GMSL time series (Church and White, 2011).

The trends over the various time periods are summarised in Table 6. The most complete comparisons are available for periods 1966 to 2009, 1990 to 2009 and 1993 to 2009 as the tide gauge-based GMSL data

finishes in 2009. For these periods the average trends of relative sea level around the coastline are 1.4 ± 0.3, 4.2 ± 0.9 and 4.5 ± 1.3 mm yr^{-1}, which become 1.6 ± 0.2, 2.4 ± 0.5 and 2.7 ± 0.6 mm yr^{-1} after removal of the signal correlated with ENSO. After further correcting for GIA and changes in atmospheric pressure, the corresponding trends are 2.1 ± 0.2, 2.9 ± 0.5 and 3.1 ± 0.6 mm yr^{-1}, comparable with the global-average rise over the same periods of 2.0 ± 0.3 and 2.5 ± 0.6 mm yr^{-1} (from tide gauges) and 3.4 ± 0.4 mm yr^{-1} (from satellite altimeters).

There is good agreement between our results (after removing the ENSO signal) and Burgette et al. (2013) who differenced adjacent time series to minimise the effects of common-mode signals on the trend estimates. This suggests that both techniques are removing a common signal that would otherwise influence the determination of underlying rates of RMSL rise. For the ten common tide gauges in the two studies analyzed over the period beginning in 1966, the mean difference in rate is 0.2 ± 0.3 mm yr^{-1}. The correspondence between the results from these very different strategies shows both methods can robustly resolve precise rates of RMSL change, and, therefore, more clearly identify the climatic origin of the dominant large-scale signal in the tide-gauge records.

The considerable variability, unless removed, significantly biases estimates of the underlying RMSL trends, particularly in shorter tide-gauge records. This leads to the question: What is the minimum record length required to determine 'long term' RMSL trends around Australia. Douglas (1991), Tsimplis and Spencer (1997), Woodworth et al. (1992), Woodworth et al. (1999), and Haigh et al. (2009) analysed datasets from different parts of the world and demonstrated that 30 and 50 years of records are required to obtain standard errors in the order of 0.5 and 0.3 mm yr^{-1}, respectively. However, the effect of serial correlation was not taken into account in these earlier studies. When including the effect of serial correlation we find that, to obtain standard errors of 0.5 mm yr^{-1} (0.3 mm yr^{-1}) record lengths of about 45 (65) and 30 (45) years are required for Fremantle and Sydney, before the coherent part of the variability is removed and about 30 (40) and 25 (35) years, after the coherent variability is removed.

Given that past changes in Australian OVMSL are similar to global-mean changes over the last 45 years, it is likely that future changes over the 21st century will be consistent with global changes. Ongoing GIA would result in RMSL changes around Australian being slightly less (between 0.2 and 0.3 mm yr^{-1}; equivalent to 1.8 to 2.7 cm between 2010 and 2100, neglecting any error in GIA models) than the global-mean changes. Another effect related to GIA is the visco-elastic and gravitational response of the Earth to modern-day ice melt (Tamisiea and Mitrovica, 2011). This is expected to increase sea levels in the Australian region by a few (perhaps 3–5) centimetres this century (Church et al., 2011b, Slangen et al., 2012). It is possible that other, as yet poorly determined, spatial patterns of sea-level rise associated with changes in ocean circulation may have regional impacts as large, or larger, than those of GIA. Analysis of long tide gauge records revealed both linear and non-linear long-term sea-level trends, so simple extrapolation is inappropriate, especially under climate change scenarios.

The detailed description of the Sydney Fort Denison tide gauge and its data (Hamon, 1987) highlights a number of uncertainties and potential problems in the earlier parts of this record. Some of these may be related to chart digitising problems and some to registration errors, both physical and in the data recording. Great care should be taken in interpreting a single long record, no matter how much care was taken with it at the time of digitisation and in post-processing. The scales of the phenomena discussed here are of the order of several hundred to thousands of kilometres (Figs. 3, 4, 5, 6 and 10), so we should not rely on single records for predicting long-term and large-spatial-scale phenomena. There is more data for a number of sites around Australia that could be digitised and made available, and doing this would improve our knowledge of the recent past and the present. Maintenance and upgrading of existing equipment and the associated infrastructure such as GPS receivers is also important. New GPS receivers are being added to the network, including installations at Fort Denison and Newcastle in 2012.

6. Conclusion

A large part of the inter-annual and decadal variability in sea level around the whole coast of Australia is coherent and highly correlated with the Southern Oscillation Index and can be represented by a single EOF. Removing this coherent variability from both tide-gauge and altimetry records around Australia significantly reduces uncertainties of sea-level trends with more uniformity in regional trends than previously reported. An assessment of the two longest tide-gauges records (Sydney, 1886–2010; Fremantle, 1897–2010) shows that the rate of rise has been non-linear in nature with both records showing large rates of rise around the 1940s, relatively stable RMSLs between 1960 and 1990 and an increased rate of rise from the early 1990s. From 1966 to 2010, when there is good coverage of most of the Australian coastline, the average Australian relative rate of rise is slower than the global mean prior to about 1985, but the mean Australian OVMSL rate from tide gauges is close to the global mean. Since 1993, MSL trends are considerably higher than the global mean around Northern Australian and similar to the global mean around southern Australia. Higher sea-level trends in northern Australia are largely associated with natural climate variability. Even after attempts to remove the effects of this natural variability, trends around most of Australia, show an increased rate of rise from the early 1990s, consistent with global mean trends.

Acknowledgements

Altimeter data was provided by NASA, CNES, NOAA and EUMETSAT. The altimeter data used was validated with support by the Australian Integrated Marine Observing System (IMOS), established by the Australian Government through the National Collaborative Research Infrastructure Strategy (NCRIS) and the Super Science Initiative. We would like to thank Simon Williams (National Oceanography Centre Liverpool, UK) for the CATS software. We would also like to thank Professor Ian Gordon and Dr Sue Finch (Statistical Consulting Centre, University of Melbourne), and other reviewers for their review comments and advice. A workshop, hosted to bring together the team to write this paper, was funded by Office of Environment and Heritage, New South Wales.

Appendix A. Supplementary data - descripton of tide-gauge data

Supplementary data to this article can be found online at http://dx.doi.org/10.1016/j.earscirev.2014.05.011.

References

Allan, R., Ansell, T., 2006. A new globally complete monthly historical gridded mean sea level pressure dataset (HadSLP2): 1850–2004. J. Clim. 19, 5816–5842. http://dx.doi.org/10.1175/JCLI3937.1.

Altamimi, Z., Collilieux, X., Métivier, L., 2011. ITRF2008: an improved solution of the international terrestrial reference frame. J. Geod. 85, 457–473.

Amin, M., 1993. Changing mean sea level and tidal constants on the west coast of Australia. Mar. Freshw. Res. 44 (6), 911–925.

Aubrey, D.G., Emery, K.O., 1986. Australia: an unstable platform for tide-gauge measurements of changing sea levels. J. Geol. 94 (5), 699–712.

Belperio, A.P., 1993. Land subsidence and sea level rise in the Port Adelaide estuary: implications for monitoring the greenhouse effect. Aust. J. Earth Sci. 40 (4), 359–368.

Bryant, E.A., Roy, P.S., Thom, B.G., 1988. Australia—an unstable platform for tide-gauge measurements of changing sea levels: a discussion. J. Geol. 96, 635–640.

Bureau of Meteorology, 2011. The Australian Baseline Sea Level Monitoring Project, Annual Sea Level Data Summary Report, July 2010 - June 2011. , published online at http://www.bom.gov.au/oceanography/projects/abslmp/rports_yearly.shtml.

Burgette, R.J., Watson, C.S., Church, J.A., White, N.T., Tregoning, P., Coleman, R., 2013. Characterizing and minimizing the effects of noise in tide gauge time series: relative and geocentric sea level rise around Australia. Geophys. J. Int. 194 (2), 719–736. http://dx.doi.org/10.1093/gji/ggt131.

Calafat, F.M., Jordà, G., 2011. A Mediterranean sea level reconstruction (1950–2008) with error budget estimates. Glob. Planet. Chang. 79 (1–2), 118–133.

Chandler, R.E., Scott, E.M., 2011. Statistical methods for Trend Detection and Analysis in the Environmental Sciences. Statistics in Practice seriesJohn Wiley and Sons Ltd. 978-0-470-01543-8,.

Church, J.A., Freeland, H.J., 1987. The energy source for the coastal-trapped waves in the Australian Coastal Experiment region. J. Phys. Oceanogr. 17 (3), 289–300.

Church, J.A., White, N.J., 2006. A 20th century acceleration in global sea-level rise. Geophys. Res. Lett. 33 (1). http://dx.doi.org/10.1029/2005GL024826.

Church, J.A., White, N.J., 2011. Sea-level rise from the late 19th to the early 21st century. Surv. Geophys. 32 (4), 585–602.

Church, J.A., Freeland, H.J., Smith, R.L., 1986a. Coastal-trapped waves on the east Australian continental shelf. Part I: Propagation of modes. J. Phys. Oceanogr. 16 (11), 1929–1943.

Church, J.A., White, N.J., Clarke, A.J., Freeland, H.J., Smith, R.L., 1986b. Coastal trapped waves on the east Australian continental shelf. Part II: Model verification. J. Phys. Oceanogr. 16 (11), 1945–1957.

Church, J.A., White, N.J., Coleman, R., Lambeck, K., Mitrovica, J.X., 2004. Estimates of the regional distribution of sea level rise over the 1950–2000 period. J. Clim. 17 (13), 2609–2625.

Church, J.A., Hunter, J.R., McInnes, K.L., White, N.J., 2006. Sea-level rise around the Australian coastline and the changing frequency of extreme sea-level events. Aust. Meteorol. Mag. 55, 253–260.

Church, J.A., Woodworth, P.L., Aarup, T., Wilson, W.S. (Eds.), 2010. Understanding Sea-Level Rise and Variability. Wiley-Blackwell Publishing, Chichester, UK. ISBN: 978-1-4443-3451-7.

Church, J.A., White, N.J., Konikow, L.F., Domingues, C.M., Cogley, C.M., Rignot, E., Gregory, J. M., 2011a. Revisiting the Earth's sea-level and energy budgets for 1961 to 2008. Geophys. Res. Lett. 38, L18601. http://dx.doi.org/10.1029/2011GL048794 http://www.agu.org/journals/gl/gl1118/2011GL048794/.

Church, J.A., Gregory, J.M., White, N.J., Platten, S.M., Mitrovica, J.X., 2011b. Understanding and projecting sea level change. Oceanography, vol. 24(2). Oceanography Society, pp. 130–143.

Church, J.A., White, N.J., Konikow, L.F., Domingues, C.M., Cogley, J.G., Rignot, E., Gregory, J. M., 2013a. Correction to Revisiting the Earth's sea-level and energy budgets for 1961 to 2008. Geophys. Res. Lett. 40, 4066.

Church, J.A., Monselesan, D., Gregory, J.M., Marzeion, B., 2013b. Evaluating the ability of process based models to project sea-level change. Environ. Res. Lett. 8 (1). http://dx.doi.org/10.1088/1748-9326/8/1/014051.

Davis, J.L., Wernicke, B.P., Tamisiea, M.E., 2012. On seasonal signals in geodetic time series. J. Geophys. Res. 117 (B1). http://dx.doi.org/10.1029/2011JB008690.

Deng, X., Griffin, D.A., Ridgway, K., Church, J.A., Featherstone, W.E., White, N.J., Cahill, M., 2011. Satellite altimetry for geodetic, oceanographic, and climate studies in the Australian region. Coastal Altimetry. Springer, Germany. ISBN: 978-3-642-12795-3, pp. 473–508.

Douglas, B.C., 1991. Global sea level rise. J. Geophys. Res. 96, 6981–6992.

Featherstone, W.E., Filmer, M.S., 2012. The north-south tilt in the Australian Height Datum is explained by the ocean's mean dynamic topography. J. Geophys. Res. 117 (C8).

Featherstone, W.E., Filmer, M.S., Penna, N.T., Morgan, L.M., Schenk, A., 2012. Anthropogenic land subsidence in the Perth Basin: challenges for its retrospective geodetic detection. J. R. Soc. West. Aust. 95, 53–62.

Feng, M., Li, Y., Meyers, G., 2004. Multidecadal variations of Fremantle sea level: footprint of climate variability in the tropical Pacific. Geophys. Res. Lett. 31 (16).

Fleming, K., Tregoning, P., Kuhn, M., Purcell, A., McQueen, H., 2012. The effect of melting land-based ice masses on sea-level around the Australian coastline. Aust. J. Earth Sci. 59 (4). http://dx.doi.org/10.1080/08120099.2012.664828.

Freeland, H.J., Boland, F.M., Church, J.A., Clarke, A.J., Forbes, A.M.G., Huyer, A., Smith, R.L., Thompson, R.O.R.Y., White, N.J., 1986. The Australian Coastal Experiment: a search for coastal-trapped waves. J. Phys. Oceanogr. 16 (7), 1230–1249.

Fu, L.L., Cazenave, A. (Eds.), 2001. Satellite Altimetry and Earth Sciences: A Handbook of Techniques and Applications. Academic Press, International Geophysics Series.

Gehrels, W.R., Woodworth, P.L., 2013. When did modern rates of sea-level rise start? Glob. Planet. Chang. 100, 263–277.

Gehrels, W.R., Callard, S.L., Moss, P.T., Marshall, W.A., Blaauw, M., Hunter, J.J., Milton, A., Garnett, M.H., 2012. Nineteenth and twentieth century sea-level changes in Tasmania and New Zealand. Earth Planet. Sci. Lett. 315–316, 94–102.

Gong, D., Wang, S., 1999. Definition of Antarctic Oscillation Index. Geophys. Res. Lett. 26, 459–462.

Gregory, J.M., White, N.J., Church, J.A., Bierkens, M.F.P., Box, J.E., van den Broeke, R., Cogley, J.G., Fettweis, X.E., Hanna, E.P., Leclercq, P.W., Marzeion, B., Oerlemans, J., Wada, Y., Wake, L.M., van de Wal, R.S.W., 2013. Twentieth-century global-mean sea-level rise: is the whole greater than the sum of the parts? J. Clim. 26, 4476–4499. http://dx.doi.org/10.1175/JCLI-D-12-00319.1.

Haigh, I.D., Nicholls, R.J., Wells, N.C., 2009. Mean sea-level trends around the English Channel over the 20th century and their wider context. Cont. Shelf Res. 29 (17), 2083–2098.

Haigh, I.D., Eliot, M., Pattiaratchi, C., Wahl, T., 2011. Regional changes in mean sea level around Western Australia between 1897 and 2008. Proceedings of the 20th Australasian Coastal and Ocean Engineering Conference, Perth, 28–30 September.

Hamon, B.V., 1966. Continental shelf waves and the effects of atmospheric pressure and wind stress on sea level. J. Geophys. Res. 71, 2883–2893.

Hamon, B.V., 1987. A Century of Tide Records: Sydney (Fort Denison) 1886–1986. Technical Report No.7. 0158-9776Flinders Institute for Atmospheric and Marine Sciences.

Han, W., Meehl, G.A., Rajagopalan, B., Fasullo, J.T., Hu, A., Lin, J., Large, W.G., Wang, J., Quan, X.-W., Trenar, L.L., Wallcraft, A., Shinoda, T., Yeage, S., 2010. Patterns of Indian Ocean sea-level change in a warming climate. Nat. Geosci. 3, 546–550. http://dx.doi.org/10.1038/ngeo901.

Hannah, J., Bell, R.G., 2012. Regional sea level trends in New Zealand. J. Geophys. Res. 117 (C1). http://dx.doi.org/10.1029/2011JC007591.

Henry, O., Prandi, P., Llovel, W., Cazenave, A., Jevrejeva, S., Stammer, D., Meyssignac, B., Koldunov, N.V., 2012. Tide gauge-based sea level variations since 1950 along the Norwegian and Russian coasts of the Arctic Ocean; contribution of the steric components. J. Geophys. Res. Oceans 117 (C6) (1978–2012).

Hill, K.L., Rintoul, S.R., Coleman, R., Ridgway, K.R., 2008. Wind forced low frequency variability of the East Australia Current. Geophys. Res. Lett. 35 (8).

Holbrook, N.J., Goodwin, I.D., McGregor, S., Molina, E., Power, S.B., 2011. ENSO to multi-decadal time scale changes in East Australian Current transports and Fort Denison sea level: oceanic Rossby waves as the connecting mechanism. Deep-Sea Res. II Top. Stud. Oceanogr. 58 (5), 547–558.

Hunter, J., Coleman, R., Pugh, D., 2003. The sea level at Port Arthur, Tasmania, from 1841 to the present. Geophys. Res. Lett. 30 (7). http://dx.doi.org/10.1029/2002GL016813.

Jevrejeva, S., Grinsted, A., Moore, J.C., Holgate, S., 2006. Nonlinear trends and multiyear cycles in sea level records. J. Geophys. Res. Oceans 111 (C9) (1978–2012).

King, M.A., Keshin, M., Whitehouse, P.L., Thomas, I.D., Milne, G., Riva, R.E., 2012. Regional biases in absolute sea-level estimates from tide gauge data due to residual unmodeled vertical land movement. Geophys. Res. Lett. 39 (14). http://dx.doi.org/10.1029/2012GL052348.

Lambeck, K., 2002. Sea level change from mid Holocene to recent time: an Australian example with global implications. Geodyn. Ser. 29, 33–50.

Merrifield, M.A., Thompson, P.R., Lander, M., 2012. Multidecadal sea level anomalies and trends in the western tropical Pacific. Geophys. Res. Lett. 39. http://dx.doi.org/10.1029/2012GL052032 (L13602).

Mitchell, W.M., Lennon, G.W., 1992. Sea Level Monitoring in the Australasian Region. Report of the International Seminar and Follow-up Study on Mean Sea Level Monitoring in Asian and Oceania Region. Japan Hydrographic Association, Tokyo (February).

Mitchell, W.M., Chittleborough, J., Ronai, B., Lennon, G.W., 2000. 'Sea Level Rise in Australia and the Pacific', in The South Pacific Sea Level and Climate Change Newsletter. Q. Newsl. 5, 10–19.

Montgomery, R.B., 1940. Report on the work of G.T. Walker. Mon. Weather Rev. 68, 1–26.

Moore, J.C., Jevrejeva, S., Grinsted, A., 2011. The historical global sea-level budget. Ann. Glaciol. 52 (59), 8–14.

Morton, R., Henderson, B.L., 2008. Estimation of nonlinear trends in water quality: an improved approach using generalized additive models. Water Resour. Res. 44 (7). http://dx.doi.org/10.1029/2007WR006191.

Newman, M., Compo, G.P., Alexander, M.A., 2003. ENSO-forced variability of the Pacific Decadal Oscillation. J. Clim. 16, 3853–3857.

Nicholls, R.J., Cazenave, A., 2010. Sea-level rise and its impact on coastal zones. Science 328 (5985), 1517–1520.

Pariwono, J.I., Bye, J.A.T., Lennon, G.W., 1986. Long-period variations of sea-level in Australasia. Geophys. J. R. Astron. Soc. 87 (1), 43–54.

Parker, D.E., Folland, C.K., Scaife, A.A., Colman, A., Knight, J., Fereday, D., Baines, P., Smith, D., 2007. Decadal to interdecadal climate variability and predictability and the background of climate change. J. Geophys. Res. Atmos. 112 (D18). http://dx.doi.org/10.1029/2007JD008411.

Permanent Service for Mean Sea Level (PSMSL), 2012. Tide Gauge Data. Retrieved 22 August 2012 from http://www.psmsl.org/data/obtaining/.

Power, S., Colman, R., 2006. Multi-year predictability in a coupled general circulation model. Clim. Dyn. 26, 247–272.

Power, S., Casey, T., Folland, C.K., Colman, A., Mehta, V., 1999. Inter-decadal modulation of the impact of ENSO on Australia. Clim. Dyn. 15, 319–323.

Preisendorfer, R.W., 1988. Principal Component Analysis in Meteorology and Oceanography. Elsevier, Amsterdam, (436 pp.).

Provis, D.G., Radok, R., 1979. Sea-level oscillations along the Australian coast. Mar. Freshw. Res. 30 (3), 295–301.

Ray, R.D., Douglas, B.C., 2011. Experiments in reconstructing twentieth-century sea levels. Prog. Oceanogr. 91, 496–515. http://dx.doi.org/10.1016/j.pocean.2011.07.021.

Saji, N.H., Goswami, B.N., Vinayachandran, P.N., Yamagata, T., 1999. A dipole mode in the tropical Indian Ocean. Nature 401, 360–363.

Sallenger Jr., A.H., Doran, K.S., Howd, P.A., 2012. Hotspot of accelerated sea-level rise on the Atlantic coast of North America. Nat. Clim. Chang. 2, 884–888. http://dx.doi.org/10.1038/nclimate1597.

Santamaría-Gómez, A., Bouin, M.N., Collilieux, X., Wöppelmann, G., 2011. Correlated errors in GPS position time series: implications for velocity estimates. J. Geophys. Res. Solid Earth 116 (B1). http://dx.doi.org/10.1029/2010jb007701 (1978–2012).

Slangen, A.B.A., Katsman, C.A., van de Wal, R.S.W., Vermeersen, L.L.A., Riva, R.E.M., 2012. Towards regional projections of twenty-first century sea-level change based on IPCC SRES scenarios. Clim. Dyn. 38 (5–6), 1191–1209. http://dx.doi.org/10.1007/s00382-011-1057-6.

Snay, R., Cline, M., Dillinger, W., Foote, R., Hilla, S., Kass, W., Soler, T., 2007. Using global positioning system-derived crustal velocities to estimate rates of absolute sea level change from North American tide gauge records. J. Geophys. Res. Solid Earth 112 (B4). http://dx.doi.org/10.1029/2006JB004606 (1978–2012).

Tamisiea, M.E., 2011. Ongoing glacial isostatic contributions to observations of sea level change. Geophys. J. Int. 186 (3), 1036–1044. http://dx.doi.org/10.1111/j.1365-246X.2011.05116.x.

Tamisiea, M.E., Mitrovica, J.X., 2011. The moving boundaries of sea level change: understanding the origins of geographic variability. Oceanography 24 (2), 24–39.

Tregoning, P., Watson, C., 2009. Atmospheric effects and spurious signals in GPS analyses. J. Geophys. Res. Solid Earth 114 (B9). http://dx.doi.org/10.1029/2009jb006344 (1978–2012).

Tregoning, P., Watson, C.S., Ramillien, G., McQueen, H., Zhang, J., 2009. Detecting hydrologic deformation using GRACE and GPS. Geophys. Res. Lett. 36 (15). http://dx.doi.org/10.1029/2009GL038718.

Trenberth, K.E., Hurrell, J.W., 1994. Decadal atmosphere–ocean variations in the Pacific. Clim. Dyn. 9 (6), 303–319.
Tsimplis, M.N., Spencer, N.E., 1997. Collection and analysis of monthly mean sea level data in the Mediterranean and the Black Sea. J. Coast. Res. 13, 534–544.
Tsimplis, M., Spada, G., Marcos, M., Flemming, N., 2011. Multi-decadal sea level trends and land movements in the Mediterranean Sea with estimates of factors perturbing tide gauge data and cumulative uncertainties. Glob. Planet. Chang. 76 (1–2), 63–76.
Tsimplis, M.N., Raicich, F., Fenoglio-Marc, L., Shaw, A.G.P., Marcos, M., Somot, S., Bergamasco, A., 2012. Recent developments in understanding sea level rise at the Adriatic coasts. Phys. Chem. Earth A/B/C 40, 59–71.
Wahl, T., Jensen, J., Frank, T., Haigh, I.D., 2011. Improved estimates of mean sea level changes in the German Bight over the last 166 years. Ocean Dyn. 61 (5), 701–705.
Wahl, T., Haigh, I.D., Woodworth, P.L., Albrecht, F., Dillingh, D., Jensen, J., Nicholls, R., Weisse, R., Wöppelmann, G., 2013. Observed mean sea level changes around the North Sea coastline from the beginning of the 19th century to the present. Earth Sci. Rev. 124. http://dx.doi.org/10.1016/j.earscirev.2013.05.003.
Walker, G.T., 1923. Correlation in seasonal variations of weather. VIII. A preliminary study of world-weather. Mem. Indian Meteorol. Dep. 24 (4), 75–131.
Watson, P.J., 2011. Is there evidence yet of acceleration in mean sea level rise around mainland Australia? J. Coast. Res. 27 (2), 368–377.
Watson, C., White, N., Church, J., Burgette, R., Tregoning, P., Coleman, R., 2011. Absolute calibration in Bass Strait, Australia: TOPEX, Jason-1 and OSTM/Jason-2. Mar. Geod. 34 (3–4), 242–260. http://dx.doi.org/10.1080/01490419.2011.584834.
Wijffels, S., Meyers, G., 2004. An intersection of oceanic waveguides: variability in the Indonesian throughflow region. J. Phys. Oceanogr. 34 (5), 1232–1253.
Williams, S.D.P., 2008. CATS: GPS coordinate time series analysis software. GPS Solutions 12 (2), 147–153.
Wolter, K., 1987. The Southern Oscillation in surface circulation and climate over the tropical Atlantic, Eastern Pacific, and Indian Oceans as captured by cluster analysis. J. Clim. Appl. Meteorol. 26 (4), 540–558.
Wood, S.N., 2006. Generalized Additive Models: An Introduction with R. Chapman & Hall/CRC 978-1-58488-474-3,.
Woodworth, P.L., Player, R., 2003. The permanent service for mean sea level: an update to the 21st century. J. Coast. Res. 19, 287–295.
Woodworth, P.L., Pugh, D.T., DeRonde, J.G., Warrick, R.G., Hannah, J. (Eds.), 1992. Sea Level Changes: Determination and Effects, vol. 69. American Geophysical Union, Washington, DC, pp. 1–196.
Woodworth, P.L., Tsimplis, M.N., Flather, R.A., Shennan, I., 1999. A review of the trends observed in British Isles mean sea level data measured by tide gauges. Geophys. J. Int. 136 (3), 651–670.
Woodworth, P.L., Teferle, R.M., Bingley, R.M., Shennan, I., Williams, S.D.P., 2009. Trends in UK mean sea level revisited. Geophys. J. Int. 176 (1), 19–30.
Woodworth, P.L., Gehrels, W.R., Nerem, R.S., 2011. Nineteenth and twentieth century changes in sea level. Oceanography 24 (2), 80–93.
Wöppelmann, G., Letetrel, C., Santamaria, A., Bouin, M.-N., Collilieux, X., Altamimi, Z., Williams, S.D.P., Martin Miguez, B., 2009. Rates of sea-level change over the past century in a geocentric reference frame. Geophys. Res. Lett. 36 (12). http://dx.doi.org/10.1029/2009GL038720.
Wunsch, C., Stammer, D., 1997. Atmospheric loading and the oceanic "inverted barometer" effect. Rev. Geophys. 35, 79–107.
You, J.-Z., Lord, D.B., Watson, P.J., 2009. Estimation of Relative Mean Sea Level Rise from Fort Denison Tide Gauge Data. Proceedings of the 19th Australasian Coastal and Ocean Engineering Conference, Wellington, New Zealand.
Zhang, X., Church, J.A., 2012. Sea level trends, interannual and decadal variability in the Pacific Ocean. Geophys. Res. Lett. 39 (21).